



HAL
open science

A 2D open-framework cadmium(II) complex templated by 1,4-bis(3-aminopropyl)piperazine: crystal structure, optical properties, theoretical and biological study

Zeineb Ouerghi, Imen Dridi, Philippe Guionneau, S. Auguste, Riadh Kefi

► To cite this version:

Zeineb Ouerghi, Imen Dridi, Philippe Guionneau, S. Auguste, Riadh Kefi. A 2D open-framework cadmium(II) complex templated by 1,4-bis(3-aminopropyl)piperazine: crystal structure, optical properties, theoretical and biological study. *Journal of the Iranian Chemical Society*, 2023, 20 (8), pp.1801-1820. 10.1007/s13738-023-02798-7. hal-04171449

HAL Id: hal-04171449

<https://hal.science/hal-04171449>

Submitted on 21 Aug 2023

HAL is a multi-disciplinary open access archive for the deposit and dissemination of scientific research documents, whether they are published or not. The documents may come from teaching and research institutions in France or abroad, or from public or private research centers.

L'archive ouverte pluridisciplinaire **HAL**, est destinée au dépôt et à la diffusion de documents scientifiques de niveau recherche, publiés ou non, émanant des établissements d'enseignement et de recherche français ou étrangers, des laboratoires publics ou privés.

A 2D-open-framework cadmium (II) complex templated by 1,4-bis(3-aminopropyl)piperazine: Crystal structure, Optical properties, theoretical and Biological study

Zeineb Ouerghi ^{[a]*}, Imen Dridi ^[b], Philippe Guionneau ^[c], Sandy Auguste ^[d], and Riadh Kefi ^[a]

^[a] Laboratoire de Chimie des Matériaux, Université de Carthage, Faculté des Sciences de Bizerte, 7021, Zarzouna, Tunisie

^[b] Laboratoire de biochimie et biologie moléculaire, Université de Carthage, Faculté des Sciences de Bizerte, 7021, Zarzouna, Tunisie

^[c] CNRS, Université de Bordeaux, Bordeaux INP, ICMCB, UMR 5026, F-33600 Pessac, France

^[d] Institut des Molécules et Matériaux du Mans (IMMM), UMR-CNRS 6283, Le Mans Université, 72085 Le Mans Cedex 9, France

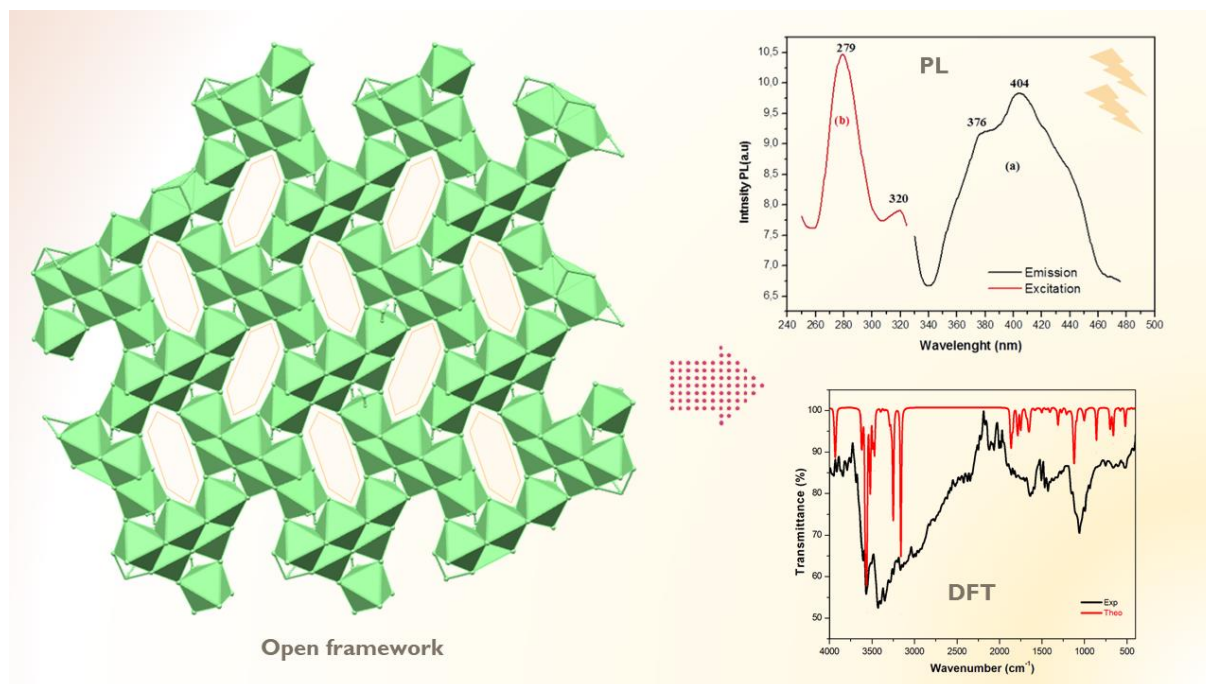
*Corresponding email: ouerghi_zeineb@yahoo.com

Abstract

A new open framework cadmium (II) complex (C₁₀N₄H₂₈)[Cd₃Cl₁₀(H₂O)].H₂O was synthesized and characterized by single-crystal X-ray diffraction. The examination of the structure shows that its atomic arrangement can be described by a covalent layered structure propagating according to the plan [101], constituted by the repetition of a motive of general formula [Cd₆Cl₂₀(H₂O)]⁸⁻. Organic groups occupy the interlayer space by establishing hydrogen bonds essentially of N–H···Cl nature. The intermolecular interactions were examined using Hirshfeld surfaces by investigating the derived 2D fingerprint plots, and enrichment ratios. The IR spectrum of the title compound was analyzed based on literature data. The optical study was investigated by UV–Vis absorption and photoluminescence. In addition to experimental data, computational investigations such as optimization, simulating the FT-IR spectrum, UV-Visible and frontiers orbital analysis of the compound were made with the Hartree-Fock method at the SDD basis set. The molecular electrostatic potential was made to evaluate reactive sites for electrophilic and nucleophilic attack for the title compound. The results from the natural bond orbital analysis were analysed in terms of hybridization of the atoms and the electronic structure of the compound. Thermal analysis showed the decomposition of the compound at 175°C.

Keywords: 2D-Open framework; Hirshfeld analysis; IR spectroscopy; Optical properties; Theoretical study; Thermal analysis

Graphical Abstract



1. Introduction

In recent years, there has been growing interest in the design and characterization of 2D open framework cadmium (II) complexes due to their intriguing structural motifs and potential applications in various fields. These complexes typically exhibit extended layers or sheets that are connected in a three-dimensional arrangement, with open spaces or channels between the layers. The unique architecture of these complexes offers opportunities for hosting guest molecules or ions in the open spaces, which can lead to applications in gas storage, separation, and sensing, among others [1-3]. Given their diverse properties, the Cd (II) complexes remain to be of particular interest among organic-inorganic hybrid compounds. They have a variety of possible coordination geometries for the metal d^{10} ion, which defines different kinds of structures, namely tetrahedral, bipyramidal trigonal, pyramidal or octahedral square and deformed polyhedral [4]. These kinds of materials have a significant worth because of their unique abilities to alter organic ligands. Inorganic polymeric anions with one-dimensional chains or two-dimensional layers are produced by the chlorocadmium (II) polymeric

compounds, a class of materials with peculiar structural frameworks. The ligands are essentially chlorine ions and water molecules if present [5-7]. Up to now, few examples of decachlorotricadmiate(II) were found in the literature presenting similar two-dimensional cadmium(II) halide network [8-11]. These compounds are used in many fields of chemistry and biology, such as medicinal chemistry [12], catalysis [13,14], photochemistry and electrochemistry [15].

The presence of organic cations which are mainly protonated amines, as spacers between the inorganic anions, obviously according to their size, confers chemical flexibility to compounds and makes it possible to modulate the distances within the chains or the layers. Especially the piperazine cycle is frequently found in biologically active compounds in several different therapeutic areas [16]. Some of these areas include antimicrobial, anticonvulsant, anti-tuberculosis, cytotoxic, antidepressant, anti-inflammatory, antimalarial, antioxidant, antiarrhythmic, and antiviral activities, etc. [17].

On the other hand, the interactions of hydrogen bonds between the protonated amino groups and the chlorine atoms of inorganic anions contribute to the formation of crystals and play a fundamental role in determining the dimensionality of the structure. Therefore, on these bases, it is possible to design structural architecture optimizing both inorganic and organic components on a molecular scale, with the desired aim of preparing compounds with unusual properties. In order to support these considerations and to attribute the factors controlling the stoichiometry and the polymeric nature of chlorocadmates (II), the possibility to synthesize and study the physical properties of these compounds has been explored in view of exploiting such a potentiality and finding new materials in electronics applications (UV-LED).

In the present investigation, we report the synthesis, crystal structure, Hirshfeld surface analysis and physicochemical characterization of a new chlorocadmiate (II) compound, whose inorganic framework is strictly two-dimensional, templated by 1,4-bis(3-aminopropyl)piperazine, and its unique features warrant further discussion.

2. Experimental

2.1 Chemical preparation

Cadmium(II) dichloride pentahydrate (6 mmol, 0.729 g) and 1,4-bis(3-aminopropyl)piperazine (0.220 g, 2 mmol) were dissolved in a concentrated HCl (4 M) solution in the presence of ethanol (15 mL) in a stoichiometric ratio. The reaction mixture of the solution was then maintained at ambient temperature. After a week, colorless parallelepiped

(C₁₀N₄H₂₈)[Cd₃Cl₁₀(H₂O)].H₂O crystals (yield 74 %) were obtained by slow evaporation with good quality for single X-ray diffraction analysis. Anal. Calc.: C, 15.87; H, 2.64; N, 7.40 %. Found: C, 15.98; H, 2.78; N, 7.22 %. The reaction equation can be schematized as follows:



2.2 X-ray data collection

A single crystal was carefully selected under a microscope in order to perform its structural analysis by X-ray diffraction. Data were collected at 150 K on a Bruker SMART APEX CCD area detector diffractometer using a mirror monochromated MoK α radiation, $\lambda = 0.71073 \text{ \AA}$. The structure was solved by a dual-space algorithm using the SHELXT program [18], and then refined with full-matrix least-square methods based on F² (SHELXL) [19]. All non-hydrogen atoms were refined with anisotropic atomic displacement parameters. H atoms were included in their calculated positions. A final refinement on F² with 5986 unique intensities and 186 parameters converged at $\omega R(F^2) = 0.105$ ($R(F) = 0.037$ for 5380 observed reflections with $I > 2\sigma(I)$). It has been checked that the unit-cell at 150 K is the same as at room temperature, exception with a small thermal contraction. Crystal data are reported in (Table 1). Drawings were made with Mercury [20].

2.3 Physical measurements

The IR spectrum was obtained using the NICOLET IR 200 FT-IR infrared spectrometer in the range of 4000–400 cm⁻¹. Solid-state absorption spectrum was registered at room temperature with a Perkin Elmer Lambda 35 UV-Vis spectrophotometer equipped with an integrating sphere in the range of 200-700 nm. The emission spectrum was recorded for the solid sample with Perkin-Elmer LS55 Spectrofluorometer at room temperature. Simultaneous Thermogravimetry (TG) and Differential Thermal Analyzer (DTA) were performed using using TG Labsys instrument operating from 28°C up to 420° C temperature at an average heating rate of 5°C/min in Argon atmosphere with a finely ground sample of 9.9 mg.

2.4 Hirshfeld Surface Analysis

Hirshfeld surface calculations were generated using the CrystalExplorer package ver.3.1.20 [21]. The X-ray single-crystal crystallographic information file of the compound was used as the input file. The normalized contact distance « d_{norm} » depends on contact distances to the closest atoms outside « d_e » and inside « d_i ». The inter-contacts shorter than the sum of the van der Waals radii are highlighted on the d_{norm} surface in red spots while contacts closer in

length or in the limit to the van der Waals radii are respectively colored in blue and white areas. The 2D fingerprint plots were generated from the Hirshfeld surface by plotting the fraction of points on the surface as a function of the pair (d_i , d_e) to summarize contact distances. The enrichment values for (x,y) and (x,x) contacts, defined as the ratio between the proportion of actual contacts C_{XY} and the theoretical proportion of random contacts R_{XY} in the crystal, were calculated using the formulas : $E_{XY} = C_{XY}/R_{XY}$ and $E_{XX} = C_{XX}/R_{XX}$. Random contacts are obtained by probability products $R_{XX} = S_X.S_X$ and $R_{XY} = 2S_X.S_Y$. The proportion S_X of a chemical type « x » on the molecular surface is obtained according to the formula $S_X = C_{XX} + \frac{1}{2} \sum_{y \neq x} C_{XY}$ [22, 23].

2.5 Computational Details

All calculations for the molecular structure were done by Gaussian 09W software [24]. Additionally, GaussView 5 software [25] was used for visualization and interpretation of all computations. Theoretical studies such as optimization, vibrational wavenumbers, UV-Vis. Spectroscopic analysis, Frontier Orbitals studies for the compound were performed using the Hartree-Fock functional method with SDD basis set level [26, 27] due to the presence of Bi atoms. The initial coordinates for the optimization process were obtained from single crystal X-ray diffraction experiment using the orpex of the compound. For UV-Vis. electronic absorption wavelengths, SDD basis set was used in the gas phase. Reduced density gradient analysis of non-covalent interactions in the molecular space of the compound were made using VMD and Multiwfn programs [28, 29].

2.6 In vitro antioxidant activity

To face the multidrug resistance of some pathogenic bacterial strains, such as *Staphylococcus aureus*, many researchers were interested in testing the antibacterial activity of natural products or chemical compounds. Many previous studies showed the efficiency Cd (II) complex as an antibacterial agent [30, 31]. Even the Cd is classified as a human carcinogen; its toxicity depends on its concentration. Indeed, the Joint Food and Agriculture Organization of the United Nations (FAO)/WHO Expert Committee on Food Additives (JECFA) established a provisional tolerable monthly intake for cadmium of 25 $\mu\text{g}/\text{kg}$ body weight [32]. The antioxidant activity of the tested compound $(\text{C}_{10}\text{N}_4\text{H}_{28})[\text{Cd}_3\text{Cl}_{10}(\text{H}_2\text{O})].\text{H}_2\text{O}$ and the 1,4-bis(3-aminopropyl)piperazine amine was evaluated using two tests DPPH (1,1-diphenyl-2-picrylhydrazyl) and ABTS (2,2'-azino-bis(3-ethylbenzothiazoline-6-sulphonic acid).

2.6.1 DPPH radical scavenging activity

The DPPH free radical scavenging assay was realized according to the protocol of [33, 34]. Briefly, different concentrations ranging between 0.5 and 50 mg/ml for TC and amine were prepared. Three milliliters of DPPH methanol solution (0.1mM) were added to 100µl of TC and amine solutions. After an incubation of 30 min of at room temperature and on the obscurity, the absorbance was measured at 517 nm. All test reactions were realized in triplicate. The scavenging activity was determined according to the following formula:

DPPH radicals scavenged activity (%) = $[(A_0 - A_1)/A_0] \times 100$. Where A_0 refers to the absorbance of the blank and A_1 refers to the absorbance measured in the presence of TC or amine.

2.6.2 ABTS radical scavenging activity

To perform the ABTS test, a stock solution was prepared by mixing an equal volume of 7 mM ABTS solution and 2.45 mM potassium persulfate. After 12 H of incubation at room temperature in the dark, an equal volume of methanol (50%) is added to the stock solution to prepare the working solution.

Different concentrations ranging between (0.5 and 100 mg/ml) for both TC and amine were prepared. Three hundred microliter of TC or amine are mixed with 3 ml of ABTS working solution. After 6 min of incubation in the dark and at room temperature, the absorbance was measured at 734 nm [35, 36]. The essay is made in triplicate. The scavenging activity was estimated based on the formula below:

ABTS radicals scavenged activity (%) = $[(A_0 - A_1)/A_0] \times 100$. Where A_0 is the absorbance of the blank (the reaction mixture without the tested compound) and A_1 is the absorbance measured in the presence of the tested compound.

2.7 Determination of *in-vitro* antibacterial activity by paper disc diffusion method

The screening of antibacterial activity of TC and amine was realized against four bacteria. The tested bacteria were one gram-positive bacteria: *Staphylococcus aureus* NCTC 6571 and three gram-negative bacteria, namely *Escherichia coli* JW 1772, *Salmonella typhimurium* ATCC w14028 and *Pseudomonas aeruginosa* SH 38 as recommended by the Clinical Laboratory Standards Institute.

Solutions (1mg/ml) of TC and amine were prepared by dissolving each of them on Dimethyl sulfoxide (DMSO). Bacteria cell suspensions were adjusted at 10^7 colony-forming units (cfu/mL). Each bacterial suspension was inoculated on nutrient agar sterile plates. Six

millimeters of diameter disks (Whatman No. 1, diameter = 6 mm) were soaked with 10 μL of TC and amine solutions. After incubation of 24 h at 37°C, inhibition zones were measured in mm. Each assay was performed in triplicate [37].

3. Results and discussion

3.1 Crystal structure

As shown in **Fig. 1(a)**, the polymeric structure contains three crystallographically independent Cd(II) ions. All the cadmium ions are octahedrally coordinated. The Cd02 cadmium ion is surrounded by five chlorine atoms and one water coordination molecule, while the remaining cadmium ions are coordinated to six chlorine atoms. Each octahedron, in the units $[\text{Cd}(02)\text{Cl}_5\text{O}]$ and $[\text{Cd}(1)\text{Cl}_6]$, shares three cis edges with neighboring octahedra while that of $[\text{Cd}(2)\text{Cl}_6]$ shares four to form $[\text{Cd}_3\text{Cl}_{10}(\text{H}_2\text{O})]^{4-}$ inorganic anions (**Fig. 1(a)**, **Fig 2(a)**). The negative charge of this anion is compensated by the organic tetra cation formed by protonating 1,4-bis(3-aminopropyl) piperazine. **Fig. 2(b)** shows that the title complex adopts a layered structure propagating according to the plan [101]. The distance between two layers is about 8.718 Å (see **Fig. 3**). They are constituted by the repetition of a motive of general formula $[\text{Cd}_6\text{Cl}_{20}(\text{H}_2\text{O})]^{8-}$ obtained by the application of an inversion center to the entity $[\text{Cd}_3\text{Cl}_{10}(\text{H}_2\text{O})]^{4-}$. Along the c axis, those pattern are connected by sharing in common the chlorine atoms Cl(4) and Cl(7) between the octahedron Cd(02) and those of the Cd1 and Cd2 belonging to a neighboring motif (**Fig. 2(c)**).

The protonated organic molecules are found in the area between the corrugated layers. The Cl11, Cl4, Cl15, Cl17 and Cl18 are bidentate bridging and Cl12 and Cl16 are tridentate, whereas Cl13 is the terminal ligand. The two linear groups (aminopropyl) of the organic part play a crucial role in the polymerization of octahedra. The Cd–Cl–Cd angles around the bridging chlorine atoms vary between 91.36(2)° and 129.65(3)° and the Cd–Cl bond lengths range from 2.5511(7) to 2.7300(7) Å, which are close to that observed in the complex in which the covalent ionic framework is in 2D [38]. The bond length Cd - O (H₂O) is 2.386 (2) is in the normal range. Indeed, this distance is in good agreement with those reported for $(\text{C}_6\text{H}_{18}\text{N}_3)[\text{Cd}_2\text{Cl}_7(\text{H}_2\text{O})].2\text{H}_2\text{O}$, in the range 2.3474 Å [39], for $(\text{C}_4\text{H}_7\text{N}_2)[\text{CdCl}_3(\text{H}_2\text{O})]$ (2.4032(2) Å) [40], and for $[\text{Cd}(\text{l}-\text{Cl})(\text{L})(\text{H}_2\text{O})]_2$ (2.407(3) Å, L = 2,2-dipyridylamine) [41]. The Cd...Cd separations of adjacent octahedra vary from 3.880 to 3.997 Å (**Table 2**). These distances are considerably longer than the values of about 3.36 Å in the linear chain structures and close to those found in a 2-D structure [38, 42].

The $[\text{C}_{10}\text{N}_4\text{H}_{28}]^{4+}$ tetra cation does not participate in coordination with the metal atom but forms ionic and hydrogen-bonded contacts with the $[\text{Cd}_3\text{Cl}_{10}(\text{H}_2\text{O})]^{4-}$ ion. All bond distances and angles within the $(\text{C}_{10}\text{N}_4\text{H}_{28})^{4+}$ ion are in good agreement with those of another complex containing the same tetracation [43, 44]. Hydrogen bonds play an important role in structural cohesion, thus the presence of water molecules in the crystal structure interferes with the interaction of protons originating whether carbon atoms or cationic nitrogen and atoms of chlorine giving rise to a network of hydrogen bonds very diverse (**Table 3**). Organic groups occupy the interlayer space by establishing hydrogen bonds essentially of nature $\text{N}-\text{H}\cdots\text{Cl}$ as shown in **Fig. 3**.

3.2 Hirshfeld surface analysis and enrichment ratios

The Hirshfeld surface analysis provides a detailed understanding of the molecular conformation and the role of various types of non-covalent interactions present between the molecules in the crystal. **Fig. 4(a)** shows the Hirshfeld surfaces mapped with d_{norm} using the asymmetric unit of the compound. It highlights the hydrogen bonding interactions represented by red spot areas related to the $\text{N}-\text{H}\cdots\text{Cl}$, $\text{O}-\text{H}\cdots\text{Cl}$ and $\text{O}-\text{H}\cdots\text{O}$ interactions.

The 2D fingerprint plots, which is a unique fingerprint for molecules in a crystal structure, is derived from the Hirshfeld surface by plotting the fraction of points on the surface as a function of the pair (d_i, d_e) as shown in **Fig. 4**, where d_i and d_e are the distances to the nearest atoms inside and outside the surface. Relative contributions to the Hirshfeld surface area for various close intermolecular contacts reveal that $\text{H}\cdots\text{Cl}$ are the dominant contacts with an average contribution of 62 % (see **Fig. 4(c)**) referring to the existing hydrogen bonds with distances $d_i + d_e$ down to 2.8 Å. The $\text{Cd}\cdots\text{Cl}$ and $\text{H}\cdots\text{H}$ contacts are also broadly distributed and constitute the most frequent interactions after the $\text{H}\cdots\text{Cl}$ contacts, respectively 17 % and 12.1 % of the total Hirshfeld surface (**Fig. 4(d,e)**). Furthermore, the crystal packing is also stabilized by $\text{Cl}\cdots\text{Cl}$ contacts with an average of 6.4 % of the surface area. Relative contributions of the various close intermolecular contacts are summarized in **Fig. 4(k)**.

The enrichment ratio of contacts between the different chemical species was calculated to identify over-represented and favored contacts in the crystal packing. They are defined as the ratio between the proportion of actual contacts (C%) in the crystal and the theoretical proportion of equi-distributed random contacts (R%) that are calculated from the corresponding surface proportions of different atoms (S%) listed in the histogram in **Fig. 4(j)**.

The enrichment (E) values are summarized in **Table 4**. If the enrichment is larger than unity $E_{xy} > 1$ for pairs of elements (x...y), then they are over-represented contacts, whereas for $E_{xy} < 1$ they are considered unfavorable contacts. The Cd...Cl and O...H contacts are the most favorable intermolecular interactions, showing an interesting enrichment ratio $E_{Cd...Cl} = 2.14$ and $E_{O...H} = 2.07$. Hens are the driving forces in the molecular arrangement in the structure. The H...Cl contacts appear with an enrichment larger than unity $E_{H...Cl} = 1.52$. They are electrostatically favorable due to the partial charges with opposite signs of Hydrogen and chloride atoms. Additionally, they are both establishing most of the surface interactions as $S_H = 44.25$ and $S_{Cl} = 46$ in the crystal. Despite the abundance of H...H contacts, they are slightly underrepresented with an enrichment ratio of $E_{H...H} = 0.61$. The structure is also characterized by significant Under-representation enrichments for Cl...Cl, O...Cl and Cd...H indicating their low significance in the crystal.

3.3 IR Absorption Spectroscopy

The experimental IR spectrum of the novel compound illustrated in **Fig. 5 (a)** was recorded in a wavelength ranging from 4000 to 400 cm^{-1} , showing the characteristic signals of the organic cation 1,4 bis (3-aminiopropyl) piperazin-1-4dium, presented in previous research work [45]. The optimized geometry of the compound with 67 atoms is shown in **Fig. 1(b)**. The simulated IR spectrum is given in **Fig. 5(b)**. There are differences between computed and experimental vibrational wavenumbers due to the use of isolated molecular forms in which inter-molecular interactions are not considered in the calculations. In addition to that, differences can arise from a combination of approximations, force field parameters, quantum mechanical effects, system complexity, and limitations of computational methods.

All the band characteristics are regrouped in **Table 5**. The band at 3436 cm^{-1} , shown in the experimental spectrum, is due to the stretching modes of the H_2O molecules, while theoretically are detected at 3900 cm^{-1} . The NH stretching vibrations of the terminal groups were calculated within 3520-2659 cm^{-1} region. Symmetric and asymmetric NH stretching modes of terminal groups were calculated at 3469 cm^{-1} and 3567 cm^{-1} , respectively. On the other hand, the NH stretching modes on the ring were computed at 3158 and 3268 cm^{-1} . Experimentally, the bands at 1611 and 1490 cm^{-1} are attributed to NH_3 asymmetric and symmetric deformation modes respectively. The appearance of the large band between 1200 and 1433 cm^{-1} correspond respectively to asymmetric and symmetric deformation of CH_2 groups. The weak peak at 1159 cm^{-1} corresponds to the deformation of N-H. The peak at 994

and 943 cm^{-1} are assigned respectively to the deformation of C–C and C–N. The vibrations from 993 to 411 cm^{-1} can be attributed to the C–C–C, C–C–N and C–N–C groups. In the computed spectrum, the terminal groups NH bending vibrations were computed at interval 1870 - 1112 cm^{-1} , while the NH bending vibration on the ring was calculated at 1691 cm^{-1} . The other CH and NH bending bands were computed at interval of 1686 - 881 cm^{-1} . Ring vibrations in the range of 748 - 496 cm^{-1} and NH₃ wagging vibrations in the range of 455 - 418 cm^{-1} were calculated.

3.4 Optical analysis and HOMO-LUMO analysis

The solid-state UV-Vis spectrum of crystalline $(\text{C}_{10}\text{N}_4\text{H}_{28})[\text{Cd}_3\text{Cl}_{10}(\text{H}_2\text{O})]\cdot\text{H}_2\text{O}$, measured at room temperature is shown in **Fig. 6(a)**. The absorption spectrum exhibits two distinct absorption bands centered at 260 and 360 nm. This is very similar to that observed for other previously reported chlorocadmite based hybrid materials [46-49]. In the case of our structure, the organic molecule does not present any chromophore, therefore it is transparent in the visible region and consequently, the observed optical absorptions derive from the transitions purely of the inorganic part.

The lowest energy absorption peak at 360 nm (3.44 eV) is mainly due to the bandgap absorption and it is assigned to the excitation of free electron–hole pairs within the $[\text{CdCl}_6]$ octahedron. This band-to-band absorption is characterized by the transition from the top of the valence band consisting of Cl (3p) orbital to the bottom of the Cd (5s) conduction band. The maximum energy absorption peak at 260 nm (4.77 eV) can be assigned to the absorption of the highest energetic level in the conduction band. It can be attributed to the excitation of free electron–hole pairs between O (2s or 2p) and Cd(5s) within $[\text{CdCl}_5(\text{H}_2\text{O})]^-$ octahedron [50]. In addition, the value of the gap energy found by the Kubelka-Munk function: $[F(R) = (1-R)^2 / 2R]$ (Tauc method [51]) is 3.2 eV (**Fig. 7**). This wide band gap is in the range of semiconductor materials [52, 53], and is consistent with values found for other cadmium halide compounds investigated as potential solar absorbers.

The UV-Vis parameters were computed with Hartree-Fock functional method, with SDD basis set. The calculated UV-Vis. spectrum is given in **Fig. 6(b)**. The percentages of main contributions for electronic transitions corresponding to the computed wavelengths were evaluated with GaussSum 3.0.1 software [54]. The computed UV-Vis. electronic absorption wavelengths, oscillation strengths and main contributions for electronic transitions are given in **Table 6**. The maximum oscillator strength value was calculated as 0.7357 and the

corresponding wavelength is 244.919 nm. The main contribution to this absorption band is due to the transition from HOMO-1 to LUMO with 41% contribution. The subsequent HOMO→LUMO+13 transition also provides a significant contribution with 49%. As it is seen **Fig. 8**, HOMO electrons are principally localized on cadmium and chloride atoms and the LUMO and LUMO+13 electrons are also located on both cadmium and chloride. In this case, it can be said that there are charge flows from cadmium orbitals to chloride atoms occurring.

The HOMO (Highest Occupied Molecular Orbital) and LUMO (Lowest Unoccupied Molecular Orbital) known FMOs (Frontier Molecular Orbitals) are used to determine the electronic transitions, charge transfers, and molecular electronic properties of molecular systems. Especially, HOMO-LUMO energy gaps give information on the chemical reactivity and stability of the molecules [55]. A small energy gap indicates more polarizable and highly chemical reactive molecules that are called soft molecules [56]. The visualization of FMOs is given in **Fig. 8**. The HOMO, LUMO and |HOMO-LUMO| gap values were computed as -7.06 eV, -0.44 eV and 6.62 eV, respectively. The chemical hardness η , the global softness S , the electron affinity ($I = -E_{\text{HOMO}}$) and the ionization potential ($A = -E_{\text{LUMO}}$). Also, the values of electronegativity determined according to the definition of Mulliken ($\chi = (I+A)/2$), the global chemical potential ($\mu = -(I+A)/2$) and the global electrophilicity introduced by Parr and al. ($\omega = \mu^2/2\eta$) are regrouped in **Table7** [57-59].

Since the family of hybrid cadmium compounds has potential applications as luminescent materials, the compound was studied under 280 nm excitation and the luminescence spectrum is illustrated in **Fig. 9(a)**. The fluorescence spectrum gives three violet emission peaks in decreasing order of energy respectively at 376, 404 and 440 nm. The two peaks at 404 and 440 nm agree well with recently reported emission peaks at around 420 nm on CdCl₄ based materials [46]. Except that the degeneration on two peaks can be explained by the coexistence of the two [CdCl₆] and [CdCl₅(H₂O)] octahedrons. The third emission peak at 376 nm is under the estimated gap energy and then can be assigned to luminescence arising from excitonic states formed within the inorganic framework (bound electron-hole pairs). On the other hand, the excitation spectrum which translates the variation of the intensity of the emission band at 380 nm as a function of the excitation wavelengths is illustrated in **Fig. 9(b)**. It shows an intense band at 279 nm.

3.5 Reduced density gradient analysis (RDG)

Crystalline solids exhibit rich and various bonding patterns. Weak interactions are of great interest because they add up and generate very strong molecule conformations. They have a unique signature, and their presence can be revealed from the electron density, and manifest in real space as low-gradient isosurfaces with low densities [60]. Weak interactions in the structure of the compound were analyzed using the RDG approaches, based on the electron density and their derivatives as developed by Johnson et al [60]. This approach gives a quick and rich visualization of van der Waals interactions, hydrogen bonds, and steric clashes, requiring only the atomic coordinates as input. The gradient isosurfaces are represented as broad regions of the real space and colored according to the corresponding values of the sign of the eigenvalue λ_2 value, which is a good indicator of the nature and the stabilizing or destabilizing character of intermolecular interactions since it characterizes density fluctuations. The sign of λ_2 distinguishes bonded ($\lambda_2 < 0$) from nonbonded ($\lambda_2 > 0$) interactions. Thus, analysis of this sign helps to discern between different types of noncovalent interactions, whereas the density itself provides information about their strength [60]. Therefore, different types of interactions can be determined just by examining the sign of λ_2 values. The positive sign ($\lambda_2 > 0$) refers to repulsive contributions corresponding to steric ring and cage effects, the negative sign ($\lambda_2 < 0$) indicates attractive regions corresponding to strong hydrogen and dipole-dipole bonds, while values near the zero indicate very weak van der Waals interactions.

Fig. 10(a) shows the color-filled isosurface of the compound and the plots of the reduced density gradient against the electron density multiplied by the second eigenvalue of the density Hessian represented as individual peaks. Plots in the $[(-0.05) - (+0.05)$ a.u] region correspond to different types of non-covalent interactions. The region in blue color corresponds to the dispersion to strong hydrogen bonds (N–H···Cl, O–H···Cl and O–H···O) and reflects the importance of these bonds in maintaining and stabilizing the three-dimensional structure of the crystal. Green plates located between the anionic and cationic entities are attributed to van der Waals interactions in the $[(-0.02) - (+0.01)]$ region **Fig. 10(b)**. Finally, the red region corresponds to repulsive interactions nearer the C-C bonds reflecting the steric effect.

3.6 Molecular electrostatic potential surface (MEPS)

MEPS analysis enables the determination of electron-donor and electron-acceptor sites in molecules, which is helpful in investigating intra and intermolecular interactions. It is related to predicting the reaction sites or attacks with potential electrophiles or nucleophiles as well as hydrogen bonding interactions. The charge distribution of the compound can be easily seen

from the different colorations of their mapped surface in **Fig. 11**. The dispersion of potential in the compound is from - 8.594 to 8.594 a.u. The area of positive potentials, which refers to a deficient in electrons, is characterized by a blue colour observed at the level of the hydrogen atoms, as expected due to its higher donor capacity, especially near the -NH^{3+} and -NH^+ groups of the piperazine cation, candidate for nucleophilic attacks. The negative electrostatic potential sites are seen on the chlorine atoms, candidate for electrophilic attacks, surrounding the Cd^{2+} cations. The yellow area colour is typical of slightly inert region which confirms the existence of $\text{N-H}\cdots\text{Cl}$ hydrogen bonding, as being a donor-acceptor interactions, between the organic cation and the inorganic part. The more the electrostatic potential of the acceptor becomes negative, the less the donor turns negative [61]. Finally, the green colour indicates the neutral zones in the compound.

3.7 Natural bond orbital analysis

The natural bond orbital (NBO) analyses were made to explore intra- and intermolecular forces in the compound. This method is very useful and gives information about interactions in both filled and virtual orbital spaces. It also reveals charge transfer or conjugative interactions in the molecular system. Delocalization of electron density between occupied Lewis-type (bond or lone pair) NBO orbitals and formally unoccupied (antibond or Rydberg) non-Lewis NBO orbitals correspond to a stabilizing donor-acceptor interactions as mentioned in **Table 8, 9**. The larger the $E^{(2)}$ value, the more intensive is the interaction between electron donors and electron acceptors. From the NBO analysis, the strong Lone Pair interactions (LP) of Cl19 with N47 - H48, Cl22 with N26 - H27, O23 with O12 - H13 and Cl6 with O12 - H14 confirms the strong intermolecular hydrogen bonding present in the structure with high stabilization energy of 20.26, 22.67, 19.61, 7.33 respectively. The second order perturbation theory analysis of Fock matrix in natural bond orbital basis indicates a displacement of the electronic doublets inside the anionic part and that the chlorine atoms participate in the transfer inside the anion through the intermediary of one of their free doublets, causing stabilization of the system.

3.8 Thermal Behavior

The thermal analysis (TG/DTA) results are reported in **Fig. 12**. It was carried out under Argon atmosphere with a heating rate of $5\text{ }^\circ\text{C}\cdot\text{min}^{-1}$ in the range of 28–420 $^\circ\text{C}$. The DTA curve shows three endothermic phenomena, located at 80, 135 and 175 $^\circ\text{C}$. the first small peak corresponds to the start of the crystallization of water molecule, with a mass loss on the TG curve very close to the theoretical value [Δm_1 (theo) = 2.38%, Δm_1 (exp) = 2.64%]. The second

large peak corresponds simultaneously to the phenomenon of dehydration of Cd(II) coordinated water molecule, and to the release of four chloride acid molecules arising from the intermolecular elimination reaction and deprotonation of the amine the decomposition of the organic part of the compound. These two phenomena are reflected on the TG curve by the loss close to that theoretical: ($\text{H}_2\text{O} + 4 \text{HCl}$: Theo 21.69 % ; exp 22.4 %). Finally, a series of endothermic peaks corresponding to the decomposition of the organic part, with remarkable weight loss observed in the TG curve and the formation of a carbon black deposit, obtained at the end of the experiment.

3.9 In vitro antioxidant activity of the title compound (TC) and the amine

The free radical scavenging activity was assessed by two standard methods (DPPH and ABTS) using a spectrophotometer for both the tested compound and amine. The *in-vitro* antioxidant activity of the amine was evaluated to access if the TC was more effective as an antioxidant or not. Results issued from both DPPH and ABTS tests showed that the scavenging activity of the TC is higher than the amine. Indeed, the IC_{50} of the TC was 98.2 ± 0.8 mg/ml in the DPPH test and 78.17 ± 1.068 mg/ml in the ABTS test. However, in both DPPH and ABTS tests, the IC_{50} of the amine was higher than 100 mg/ml. The TC can be used as a free radical scavenger substance (**Fig. 13**).

3.10 Determination of antibacterial activity by disc diffusion method

The antibacterial activity of the amine was tested to identify if the TC was more effective as an antibacterial agent against the tested bacteria or not. The antibacterial activity of TC and amine dissolved in Dimethyl sulfoxide (DMSO) (1 mg/mL) was accessed by the disc diffusion method (**Fig. 14**). Results showed that the diameter of inhibition caused by TC or amine didn't depend on the membrane structure of the tested bacteria (gram-positive or gram-negative) (**Table 10**). The amine was not effective against any of the tested bacteria (The inhibition diameter was equal to the disc area (6mm)). Nevertheless, the TC antibacterial activity depended on the tested bacteria. Indeed, the largest inhibition diameter (10 ± 0.33 mm) was recorded in *Staphylococcus aureus* NCTC 6571. However, the smallest inhibition diameter (6mm) was recorded in *Salmonella typhimurium* ATCC 14028.

4. Conclusion

In summary, this paper reports the synthesis and the study of some properties of a 2D chlorocadmate(II) compound: $(C_{10}N_4H_{28})[Cd_3Cl_{10}(H_2O)] \cdot H_2O$. Its atomic arrangement can be described by a covalent layered structure propagating according to the plan [101]. The intermolecular interactions that led to the molecular packing were investigated by the Hirshfeld surface which revealed the presence of $Cl \cdots Cl$ interactions. Vibrational study showed the characteristic absorption peaks of different functional groups present in the compound. The optical properties revealed the luminescent character of the material. In addition to experimental studies, quantum mechanical calculations have been made on the structure. The vibrational frequencies were compared with experimental ones. UV-Vis. data and Frontier Orbitals were evaluated simultaneously to support each other. When the experimental data is compared with calculated ones, it can be easily seen that there is slightly different each other. It is well known that the experimental results belong to solid phase of molecules, while the theoretical results are related to the gas phase of the isolated molecules. The differences between the calculated and experimental data are due to the use of isolated molecular forms that do not take into account intermolecular interactions in the calculations. Plotting low-gradient isosurfaces allows real-space visualization of noncovalent interactions. Large, negative values of sign $(\lambda_2)\rho$ are indicative of attractive interactions (such as dipole-dipole or hydrogen bonding); while if sign $(\lambda_2)\rho$ is large and positive, the interaction is nonbonding. Values near zero indicate very weak, van der Waals interactions. The NBO analysis has provided detailed insights into the nature of bonding in the compound. The thermal analysis revealed that the compound maintains stable up to 175 °C. The biological study indicated that the title compound may be used as a free radical scavenger substance.

Supplementary data

Crystallographic data of the structure have been deposited in the Cambridge Crystallographic data center CCDC 2043955. These data can be obtained free of charge via www.ccdc.cam.ac.uk/data_request/cif.

Conflict of interest

The authors declare there is no conflicts of interest to declare that are relevant to the content of this article.

References

- [1] R-Q. Zou, X-H. Bu, and R-H. Zhang, Novel Eclipsed 2D Cadmium(II) Coordination Polymers with Open-Channel Structure Constructed from Terephthalate and 3-(2-Pyridyl)pyrazole: Crystal Structures, Emission Properties, and Inclusion of Guest Molecules, *Inorg. Chem.* 43 (2004) 5382–5386. <https://doi.org/10.1021/ic049625e>.
- [2] R. Vaidhyanathan, Srinivasan Natarajan, and C. N. R. Rao, Open-Framework Cadmium Succinates of Different Dimensionalities, *Inorg. Chem.* 41 (2002) 5226–5234. <https://10.1021/ic020333s>.
- [3] B. Ding, L. Yi, Y. Wang, P. Cheng, D-Z. Liao, S-P. Yan, Z-H. Jiang, H-B. Song and H-G. Wang, Synthesis of a series of 4-pyridyl-1,2,4-triazole-containing cadmium(II) luminescent complexes, *Dalton Trans.* (2006) 665–675. <https://doi.org/10.1039/B508332J>.
- [4] P.S. Subramanian, D. Srinivas, Synthesis, spectral characterization and magnetic properties of dicarboxylato-bridged dinuclear copper(II) complexes with n-pyridylsalicylidenaminato ligand, *Polyhedron.* 15 (1996) 985-989. [https://doi.org/10.1016/0277-5387\(95\)00307-X](https://doi.org/10.1016/0277-5387(95)00307-X).
- [5] A.A. Khandar, F.A. Afkhami, S.A. Hosseini-Yazdi, J. Lipkowski, W.G. Dougherty, W.S. Kassel, H.R. Prieto, S. García-Granda, Synthesis, Characterization and Crystal Structure of Zn(II) and Cd(II) One- and Two-Dimensional Coordination Polymers Derived from Pyridine Based Schiff Base ligand, *J. Inorg. Organomet. Polym Mater.* 25 (2015) 860-868. [https://DOI: 10.1007/s10904-015-0175-8](https://DOI:10.1007/s10904-015-0175-8).
- [6] G-L. Wen, M-R. Hua, X-L. Wang, D-F. Liu, Y-H. Chen, D. Tian, Synthesis and Fluorescent Properties of a Chiral 2D Tetranuclear Cd(II) Coordination Polymer Based on Asymmetrical Biphenyltetracarboxylate, *J. Inorg. Organomet. Polym Mater.* 26 (2016) 472-478. <https://doi.org/10.1007/s10904-016-0337-3>.
- [7] Y-Q. Mu, D-S. Li, L. Bai, J-J. Yang, Y-P. Duan, J. Zhao, Characterization and Synthesis of Two New ZnII and CdII-Coordination Polymers Based on 3,3'-Biphenyl Dicarboxylate and N,N'-Donor Co-ligands, *J. Inorg. Organomet. Polym Mater.* 23 (2013) 652-658. <https://doi.org/10.1007/s10904-013-9828-7>.
- [8] A. Gagor, A. Waskowsk, Z. Czaplá, and S. Dackoc, Structural phase transitions in tetra(isopropyl-ammonium) decachlorotricadmiate(II), [(CH₃)₂CHNH₃]₄Cd₃Cl₁₀, crystal with a two-dimensional cadmium(II) halide network, *Acta Cryst. B* 67 (2011) 122–129. [https://DOI: 10.1107/S0108768110054583](https://DOI:10.1107/S0108768110054583).

[9] J-M. Xiao, catena-Poly[bis[1-chloromethyl-1,4-diazoniabicyclo [2.2.2]octane] [cadmium(II)-tri-1-chlorido-[chloridocadmium(II)]-di-1-chlorido-[chloridocadmium(II)]-tri-1-chlorido] tetrahydrate], Acta Cryst. C66 (2010) m348–m350. <https://10.1107/s0108270110040813>.

[10] S. Hermi, M. G. Althobaiti, A. A. Alotaibi, A. H. Almarri, W. Fujita, F. Lefebvre, C. Ben Nasr and M. H. Mrad, Synthesis, Crystal Structure, DFT Theoretical Calculation and Physico-Chemical Characterization of a New Complex Material (C₆H₈Cl₂N₂)₂[Cd₃Cl₁₀].6H₂O, Crystals 11 (2021) 553. <https://doi.org/10.3390/cryst11050553>.

[11] W-Q. Liao, G-Q. Mei, H-Y. Ye, Y-X. Mei, and Y. Zhang, Structural Phase Transitions of a Layered Organic–Inorganic Hybrid Compound: Tetra(cyclopentylammonium) Decachlorotricadmiate(II), [C₅H₉NH₃]₄Cd₃Cl₁₀, Inorg. Chem. 53 (2014) 8913–8918. <https://dx.doi.org/10.1021/ic500554z>.

[12] N. Farrell, Catalysis by Metal Complexes, Springer, Dordrecht, 1989, 11.

[13] K.C. Gupta, A.K Sutar, Catalytic Activities of Schiff Base Transition Metal Complexes, Coord. Chem. Rev. 252 (2008) 1420-1450. <http://dx.doi.org/10.1016/j.ccr.2007.09.005>.

[14] Y.N. Belokon, W. Clegg, R.W. Harrington, M. North, C. Young, In Situ Formation of Heterobimetallic Salen Complexes Containing Titanium and/or Vanadium Ions, Inorg. Chem. 47 (2008) 3801-3814. <https://doi.org/10.1021/ic702451a>.

[15] V. Balzani, A. Juris, M. Venturi, S. Campagna, S. Serroni, Luminescent and Redox-Active Polynuclear Transition Metal Complexes, Chem. Rev. 96 (1996) 759-834. <https://doi.org/10.1021/cr941154y>.

[16] J. Faist, W. Seebacher, R. Saf, R. Brun, M. Kaiser, R. Weis, New N-methylpiperazinyl derivatives of bicyclic antiprotozoal compounds, Eur. J. Med. Chem. 47 (2012) 510-519. <https://doi.org/10.1016/j.ejmech.2011.11.022>.

[17] K. Kulig, J. Sapa, D. Maciag, B. Filipek, B. Malawska, Synthesis and Pharmacological Evaluation of New 1-[3-(4-Arylpiperazin-1-yl)-2-hydroxypropyl]-pyrrolidin-2-one Derivatives with Anti-arrhythmic, Hypotensive, and α -Adrenolytic Activity, Arch. Pharm. Chem. Life Sci. 340 (2007) 466-475. <https://doi.org/10.1002/ardp.200700039>.

- [18] G. M. Sheldrick, SHELXT – Integrated space-group and crystal structure determination, *Acta Cryst. A* 71 (2015) 3-8. <https://doi.org/10.1107/S2053273314026370>.
- [19] G.M. Sheldrick, Crystal structure refinement with SHELXL, *Acta Cryst. C* 71 (2015) 3-8. <https://doi.org/10.1107/S2053229614024218>.
- [20] C.F. Macrae, I. Sovago, S.J. Cottrell, P.T.A. Galek, P. McCabe, E. Pidcock, M. Platings, G.P. Shields, J.S. Stevens, M. Towler, P.A. Wood, Mercury 4.0: from visualization to analysis, design prediction, *J. Appl. Crystallogr.* 53 (2020) 226-235. [https://DOI: 10.1107/S1600576719014092](https://DOI:10.1107/S1600576719014092).
- [21] S.K. Wolff, D.J. Grimwood, J.J. McKinnon, M.J. Turner, D. Jayatilaka, M.A. Spackman, CrystalExplorer. University of Western Australia, Perth, 2012.
- [22] Z. Ouerghi, T. Roisnel, R. Fezai, R. Kefi, Physico-chemical characterization, Hirshfeld surface analysis and opto-electric properties of a new hybrid material: Tris (2-amino-5-chloropyridinium) hexachlorobismuthate(III), *J. Mol. Struct.* 1173 (2018) 439-447.
- [23] C. Jelsch, K. Ejsmont, L. Huder, The enrichment ratio of atomic contacts in crystals, an indicator derived from the Hirshfeld surface analysis, *IUCrJ.* 1 (2014) 119-128. <https://doi.org/10.1107/S2052252514003327>.
- [24] J. Frisch, G. W. Trucks, H. B. Schlegel, G. E. Scuseria, et al., Gaussian 09, Revision A.02, M. Gaussian, Inc., Wallingford CT, 2009.
- [25] A.B. Nielsen, A.J. Holder, Gauss View 5.0, User's Reference, GAUSSIAN Inc., Pittsburgh, PA, 2008.
- [26] A.D. Becke, Density-functional exchange-energy approximation with correct asymptotic behavior, *Phys. Rev. A* 38 (1988) 3098-3100. <https://doi.org/10.1103/PhysRevA.38.3098>.
- [27] C. Lee, W. Yang, R.G. Parr, Development of the Colle-Salvetti correlation-energy formula into a functional of the electron density, *Phys. Rev. B* 37 (1988) 785-789. <https://doi.org/10.1103/PhysRevB.37.785>.
- [28] W. Humphrey, A. Dalke, K. Schulten, VMD: Visual molecular dynamics, *J. Mol. Graph.* 14 (1996) 33-38. [https://doi.org/10.1016/0263-7855\(96\)00018-5](https://doi.org/10.1016/0263-7855(96)00018-5).

- [29] T. Lu, F. Chen, Multiwfn: A multifunctional wavefunction analyzer, *J. Comput. Chem.* 33 (2012) 580-592. DOI: 10.1002/jcc.22885.
- [30] A. Beheshti, K. Nozarian, N. Ghamari, P. Mayer, H. Motamedi, Selective high capacity adsorption of Congo red, luminescence and antibacterial assessment of two new cadmium(II) coordination polymers, *J. Solid State Chem.* 258 (2018) 618-627. <https://doi.org/10.1016/j.jssc.2017.11.035>.
- [31] T. Kondori, N. Akbarzadeh-T, K. Abdi, M. Dusek, V. Eigner. A novel cadmium(II) complex of bipyridine derivative: synthesis, X-ray crystal structure, DNA-binding and antibacterial activities, *J. Biomol. Struct. Dyn.* 38 (2020) 236-247. <https://doi.org/10.1080/07391102.2019.1570867>.
- [32] World health organization (WHO) .2011. Geneva, World Health Organization (WHO Food Additives Series.64: 305-380.
- [33] A.C. Dhieb, I. Dridi, M. Mathlouthi, M. Rzaigui, W. Smirani, Structural Physico Chemical Studies and Biological Analyses of a Cadmium Cluster Complex, *J. Cluster Sci.* 29 (6) (2018) 1123-1131. <https://doi.org/10.1007/s10876-018-1427-x>.
- [34] A. Chinthamreddy, R. Karreddula, G.K. Pitchika, M.S. SurendraBabu. Synthesis, Characterization of [Co(BDC)(Phen)H₂O] and [Co(BDC)(DABCO)] MOFs, π .. π Interactions, Hirshfeld Surface Analysis and Biological Activity, *J. Inorg. Organomet. Polym. Mater.* 31 (2021) 1381–1394. <https://doi.org/10.1007/s10904-020-01800-6>.
- [35] A. Hachani, I. Dridi, S. Elleuch, T. Roisnel, R. Kefi, Crystal structure, spectroscopic and biological study of a new inorganic-organic hybrid compound [Cd₄Cl₁₂(H₂O)₂]_n (C₁₀N₄H₂₈)_n, *Inorg. Chem. Commun.* 100 (2019) 134-143. <https://doi.org/10.1016/j.inoche.2018.12.006>.
- [36] B.R. Krishnan, M. Ramesh, M. Selvakumar, S. Karthick, A. Sasikumar, D.V. Geerthi, N. Senthilkumar, A Facile Green Approach of Cone-like ZnO NSs Synthesized Via *Jatropha gossypifolia* Leaves Extract for Photocatalytic and Biological Activity, *J. Inorg. Organomet. Polym. Mater.* 30 (2020) 4441-4451. <https://doi.org/10.1007/s10904-020-01576-9>.
- [37] Z. Ouerghi, H. Gornitzka, E. Temel, I. Dridi, R. Kefi, A new non-centrosymmetric Chlorobismuthate(III) hybrid material: Crystal structure, optical properties and antibacterial study, *J. Mol. Struct.* 1181 (2019) 338-347. <https://doi.org/10.1016/j.molstruc.2018.12.108>.

[38] S. Soudani, J.X. Mi, F. Lefebvre, C. Jelsch, C.B. Nasr, Synthesis and physico-chemical studies of a novel layered structure with a heptanuclear Cd complex: $(C_9N_4H_{28})Cd_7(H_2O)_2Cl_{18} \cdot nH_2O (n = 5.89)$ *J. Mol. Struct.* 1084 (2015) 46-54. <https://doi.org/10.1016/j.molstruc.2014.12.007>.

[39] M. Hajji, A. Gharbi, T. Guerfel, Synthesis, Crystal Structure, Vibrational Spectra, Optical Properties and Thermal Analysis of a New Chlorocadmite Templated by 1-(2-Ammoniummethyl) Piperazinium, *J. Inorg. Organomet. Polym.* 24 (2014) 766-775. <https://doi.org/10.1007/s10904-014-0034-z>.

[40] M.S. Lassoued, W.B. Soltan, M.S.M. Abdelbaky, S. Ammar, A. Gadri, A.B. Salah, S.G. Granda, Structural, vibrational and optical properties of a new self assembled organic-inorganic crystal $(C_4H_7N_2) [CdCl_3(H_2O)]$, *J. Mater Sci: Mater Electron.* 28 (2017) 12698-12710. <https://doi.org/10.1007/s10854-017-7095-z>.

[41] J. Pickardt, B. Staub, Metallkomplexe mit 2,2'-Dipyridylamin als Liganden: Kristallstrukturen der Komplexe mit CdX_2 ($X = Cl, Br, I$) und $CuCN$ / Metal Complexes with 2,2'-Dipyridylamine as Ligand: Crystal Structures of the Complexes with CdX_2 ($X = Cl, Br, I$) and $CuCN$, *Z. Naturforsch B: J. Chem. Sci.* 54 (1999) 329-336. <https://doi.org/10.1515/znb-1999-0306>.

[42] H.L. Jiang, J.G. Mao, $[Cd_2(Te_6O_{13})][Cd_2Cl_6]$ and $Cd_7Cl_8(Te_7O_{17})$: Novel Tellurium(IV) Oxide Slabs and Unusual Cadmium Chloride Architectures, *Inorg. Chem.* 45 (2006) 717-721. <https://doi.org/10.1021/ic051703q>.

[43] S. Vetrivel, E. Vinoth, R.U. Mullai, R. Aruljothia, M.N. Mohideen, Crystal structure of 1,4-bis-(3-ammonio-prop-yl)piperazine-1,4-dium bis-[dichromate(VI)], *Acta Cryst.* E72 (2016) 616-619. <https://doi.org/10.1107/S2056989016005284>.

[44] I. Baccar, F. Issaoui, F. Zouari, M. Hussein, E. Dhahri, M.A. Valente, Magneto-structural studies of the bis (1,4-bis (3-aminopropylamine) piperazinium) chloride pentachlorocuprate (II) trihydrate, *Solid State Commun.* 150 (2010) 2005-2010. <https://doi.org/10.1016/j.ssc.2010.08.018>.

[45] M.B.M.Y. Ang, S. Huang, M. Chang, C. Lai, H. Tsai, W. Hung, C. Hu, K. Lee, Ultraviolet-initiated graft polymerization of acrylic acid onto thin-film polyamide surface for improved

ethanol dehydration performance of pervaporation membranes, *S. Purif. Technol.* 235 (2020) 116155. <https://doi.org/10.1016/j.seppur.2019.116155>.

[46] A.C. Dhieb, A. Valkonen, M. Rzaigui, W. Smirani, Synthesis, crystal structure, physico-chemical characterization and dielectric properties of a new hybrid material, 1-Ethylpiperazine-1,4-dium tetrachlorocadmate, *J. Mol. Struct.* 1102 (2015) 50-56. <https://doi.org/10.1016/j.molstruc.2015.08.044>.

[47] I. Lahbib, M. Rzaigui, W. Sta, Synthesis, crystal structure, spectroscopic, thermal and dielectric properties of a novel semi-organic pentachloroantimonate (III), *J. Mol. Struct.* 1120 (2016) 250-258. <https://doi.org/10.1016/j.molstruc.2016.04.095>.

[48] K. Boopathi, S. Moorthy Babu, R. Jagan, P. Ramasamy, Synthesis, crystal structure and growth of a new inorganic- organic hybrid compound for nonlinear optical applications: Aquadiiodo (3-aminopropanoic acid) cadmium (II), *J. Phys. Chem. Solids.* 111 (2017) 419-430. <https://doi.org/10.1016/j.jpcs.2017.08.038>.

[49] Y. Baklouti, N. Chaari, H. Feki, N.C. Boudjada, F. Zouari, Crystal structure, vibrational studies, optical properties and DFT calculations of 2-amino-5-diethyl-aminopentanium tetrachlorocadmate (II), *Spectrochim. Acta, Part A.* 136 (2015) 397-404. <https://doi.org/10.1016/j.saa.2014.09.049>.

[50] Z. Dega-Szafran, A. Katrusiak, M. Szafran, Experimental and theoretical studies of 4-hydroxy-1-methylpiperidinium perchlorate, *J. Mol. Struct.* 889 (2008) 344-351. <https://doi.org/10.1016/j.molstruc.2008.02.018>.

[51] H. Sies, Oxidative stress: oxidants and antioxidants, *Exp. Physiol.* 82 (1997) 291-295. <https://DOI: 10.1113/expphysiol.1997.sp004024>

[52] Z. Ouerghi, I. Dridi, T. Roisnel, R. Kefi, Crystal structure, optical properties, vibrational, thermal and biological study of a new polymeric Cd(II) hybrid material, *J. Mol. Struct.* 1242 (2021) 130721. <https://doi.org/10.1016/j.molstruc.2021.130721>.

[53] M.S. Lassoued, W.B. Soltan, M.S.M. Abdelbaky, S. Ammar, A. Gadri, A.B. Salah, S.G. Granda, Structural, vibrational and optical properties of a new self assembled organic-inorganic crystal (C₄H₇N₂) [CdCl₃(H₂O)], *J. Mater. Sci: Mater. Electron.* 28 (2017) 12698-12710. <https://doi.org/10.1007/s10854-017-7095-z>.

- [54] N. M. O'Boyle, A. L. Tenderholt, K. M. Langner. Software News and Updates cclib: A Library for Package-Independent Computational Chemistry Algorithms, *J. Comp. Chem.* 29 (2008) 839-845. <https://doi.org/10.1002/jcc.20823>.
- [55] I. Fleming, *Frontier Orbitals and Organic Chemical Reactio*, 1st ed., John Wiley & Sons, 1976.
- [56] K. Fukui, Role of frontier orbitals in chemical reactions, *Science*, 218 (1982) 747. <https://DOI: 10.1126/science.218.4574.747>.
- [57] W. Kohn, A. Becke, R. Parr, Density Functional Theory of Electronic Structure, *J. Phys. Chem.* 100 (1996) 12974-12980. <https://doi.org/10.1021/jp960669l>.
- [58] R.G. Parr, R.G. Pearson, Absolute hardness: companion parameter to absolute electronegativity, *J. Am. Chem. Soc.* 105 (1983) 7512–7516. <https://doi.org/10.1021/ja00364a005>.
- [59] R.G. Pearson, Absolute electronegativity and hardness correlated with molecular orbital theory, *Proc. Natl. Acad. Sci. U. S. A.* 83 (1986) 8440-8441. <https://doi: 10.1073/pnas.83.22.8440>.
- [60] E.R. Johnson, Shahar Keinan, P. Mori-Sanchez, J. Contreras-Garcia, A. J. Cohen, W. Yang. Revealing Noncovalent Interactions, *J. AM. CHEM. SOC.* 132 (2010) 6498–6506. <https://doi.org/10.1021/ja100936w>.
- [61] N. Mohan, C.H. Suresh, A Molecular Electrostatic Potential Analysis of Hydrogen, Halogen, and Dihydrogen Bonds, *J. Phys. Chem.* 118 (2014) 1697-1705. <https://doi.org/10.1021/jp4115699>.

Figures

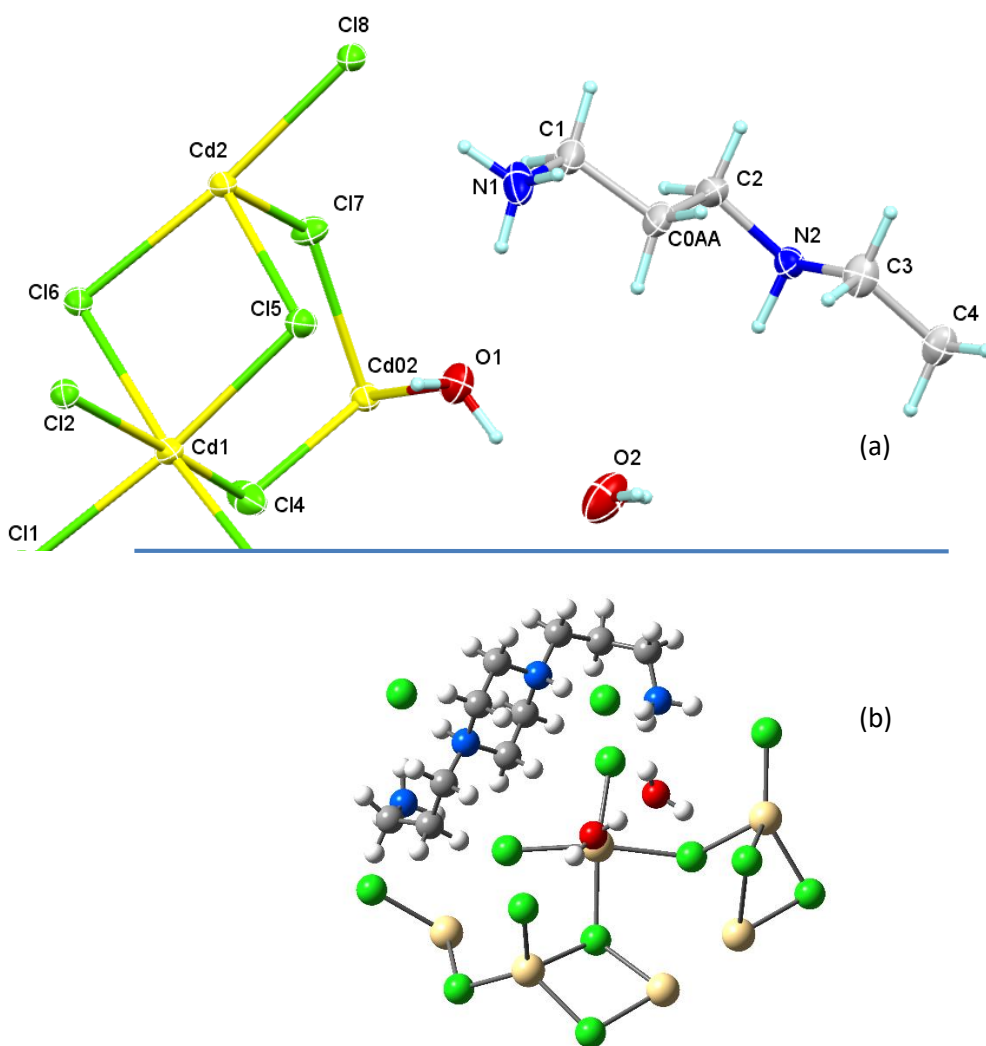


Fig. 1(a) Asymmetric unit of $(C_{10}N_4H_{28})[Cd_3Cl_{10}(H_2O)] \cdot H_2O$, with displacement ellipsoids drawn at the 50% probability level (i: -x, -y, -z). **(b)** Optimized geometry of the compound.

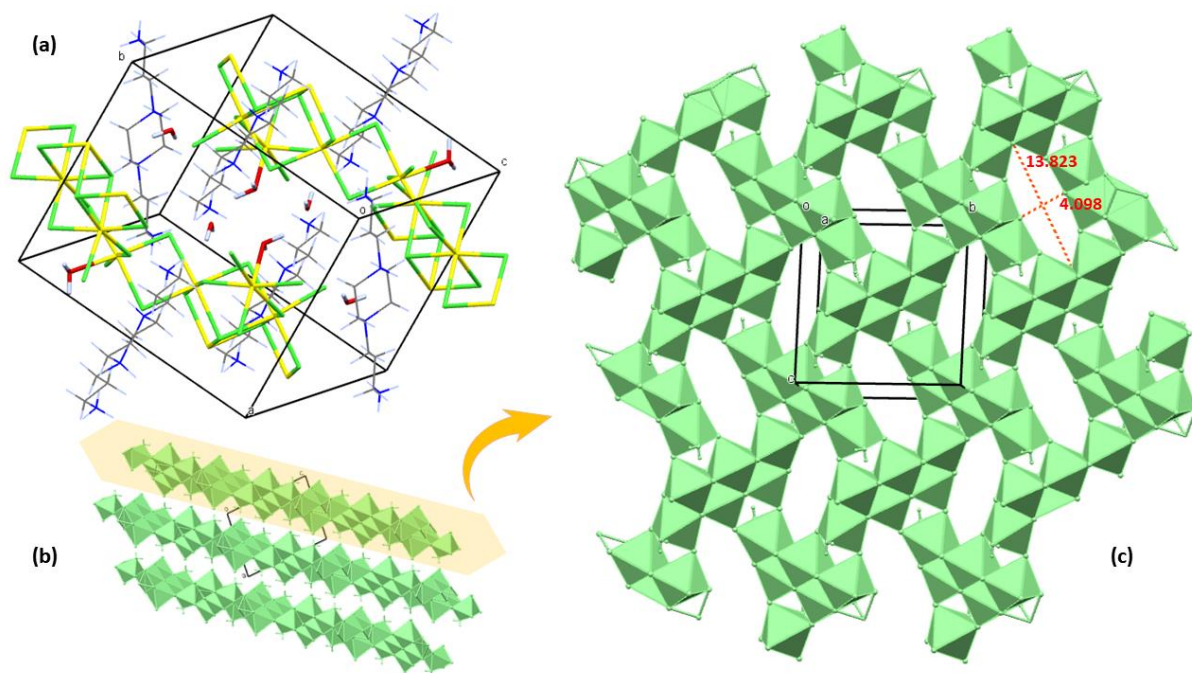


Fig. 2 (a) Perspective view of the compound; (b) Projection of the anionic part along the b axis; (c) A view of one layer of the anionic part.

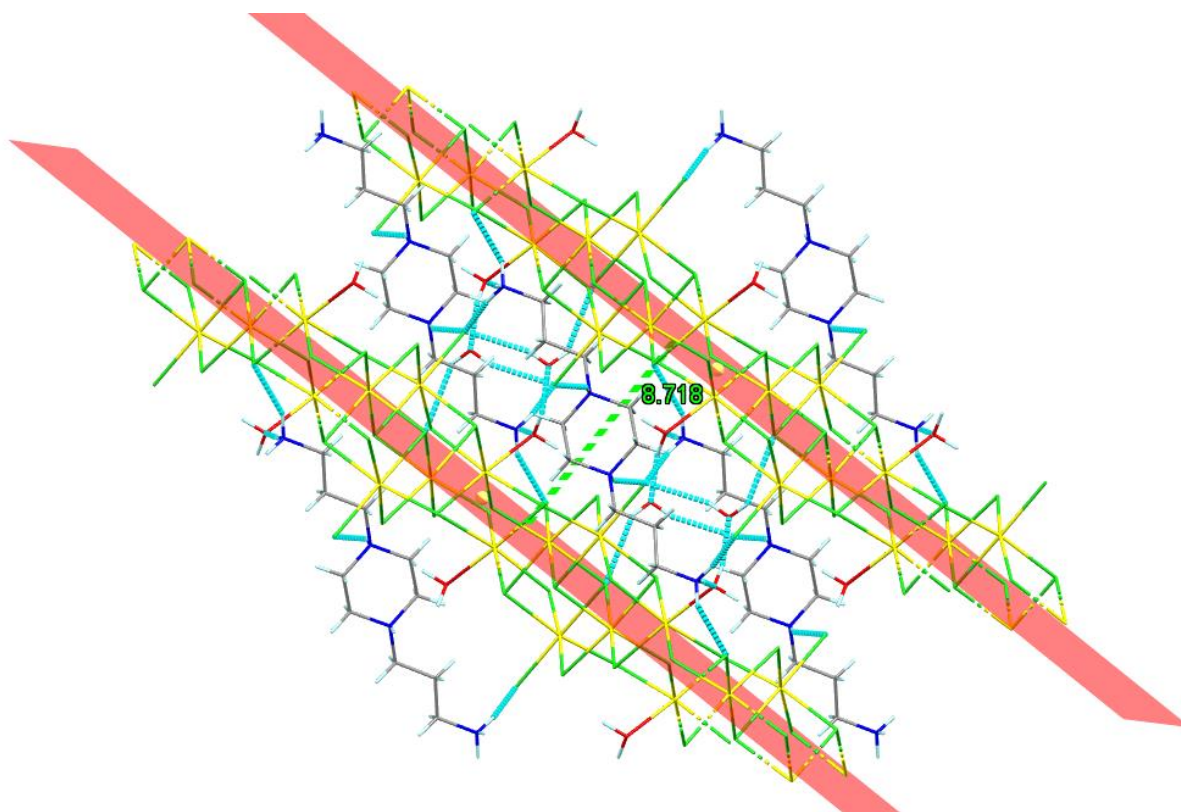


Fig. 3 Projection of the packing along the b axis showing different hydrogen bonds.

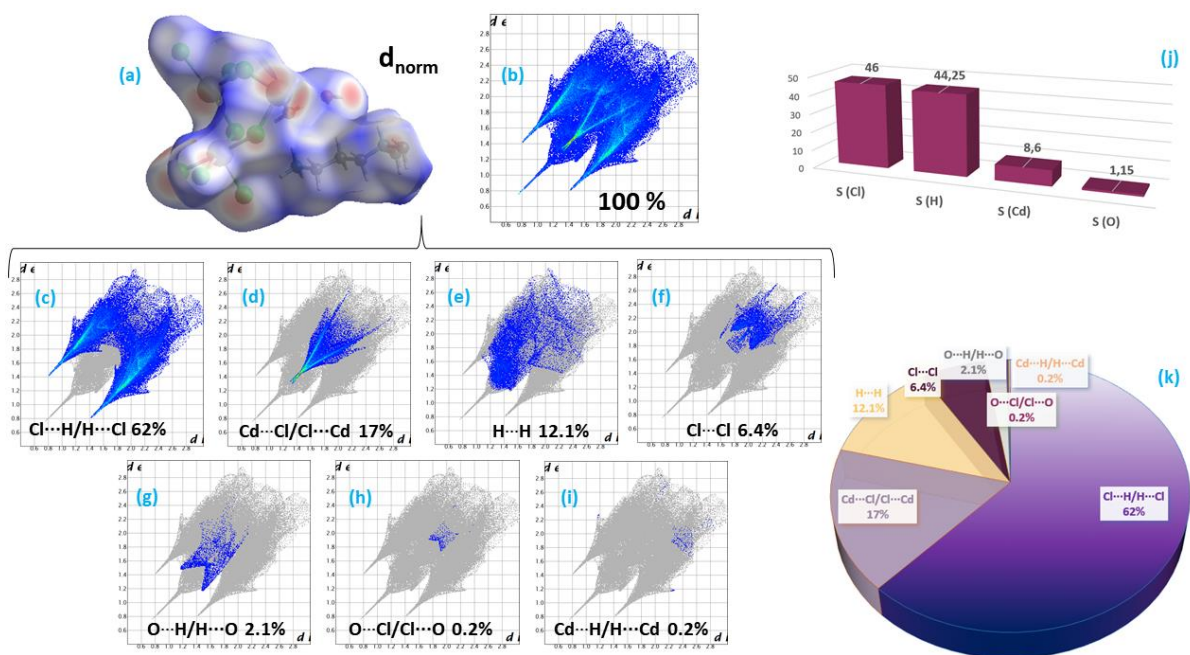


Fig. 4 (a) Hirshfeld surfaces mapped with d_{norm} shown as transparent to allow visualization of the orientation of the asymmetric unit; (b-i) 2D fingerprint plots generated from the different intermolecular interactions in the crystal; (j) Histogram of surface proportions of the different atoms in the crystal; (k) Relative contribution of various close intermolecular contacts.

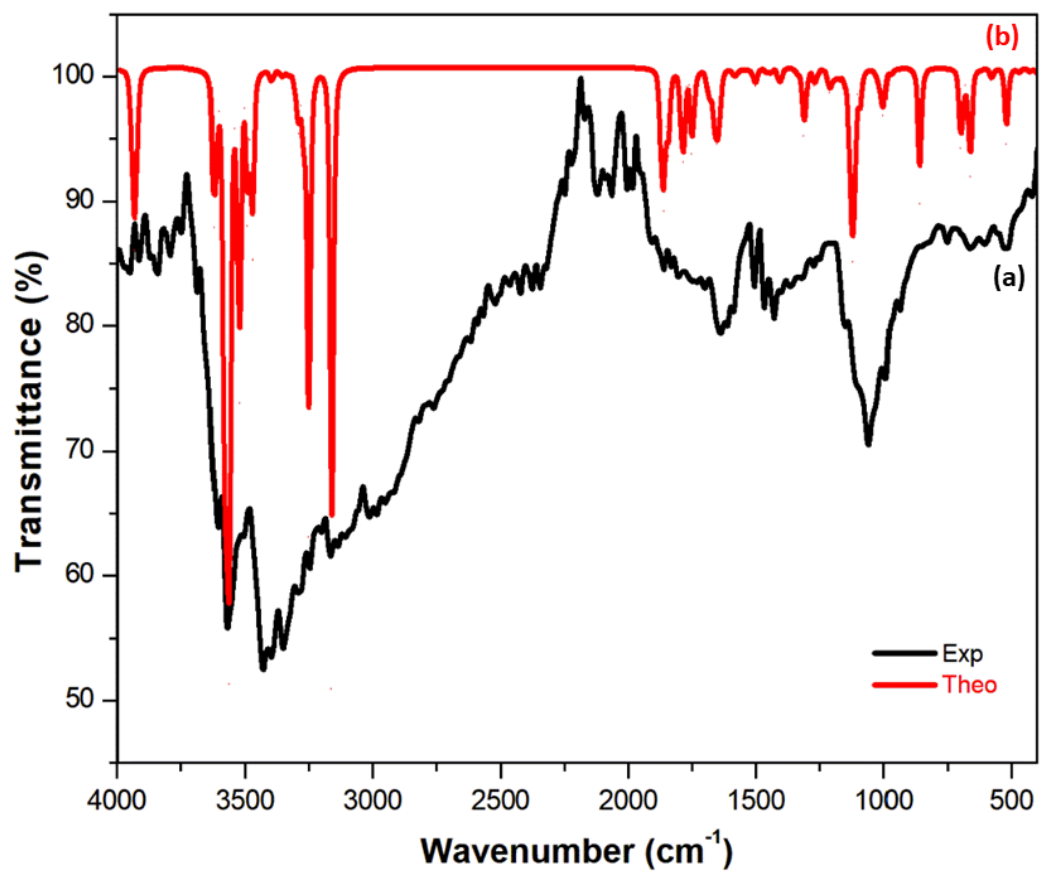


Fig. 5 Experimental (a) and theoretical (b) Infrared spectra of the compound.

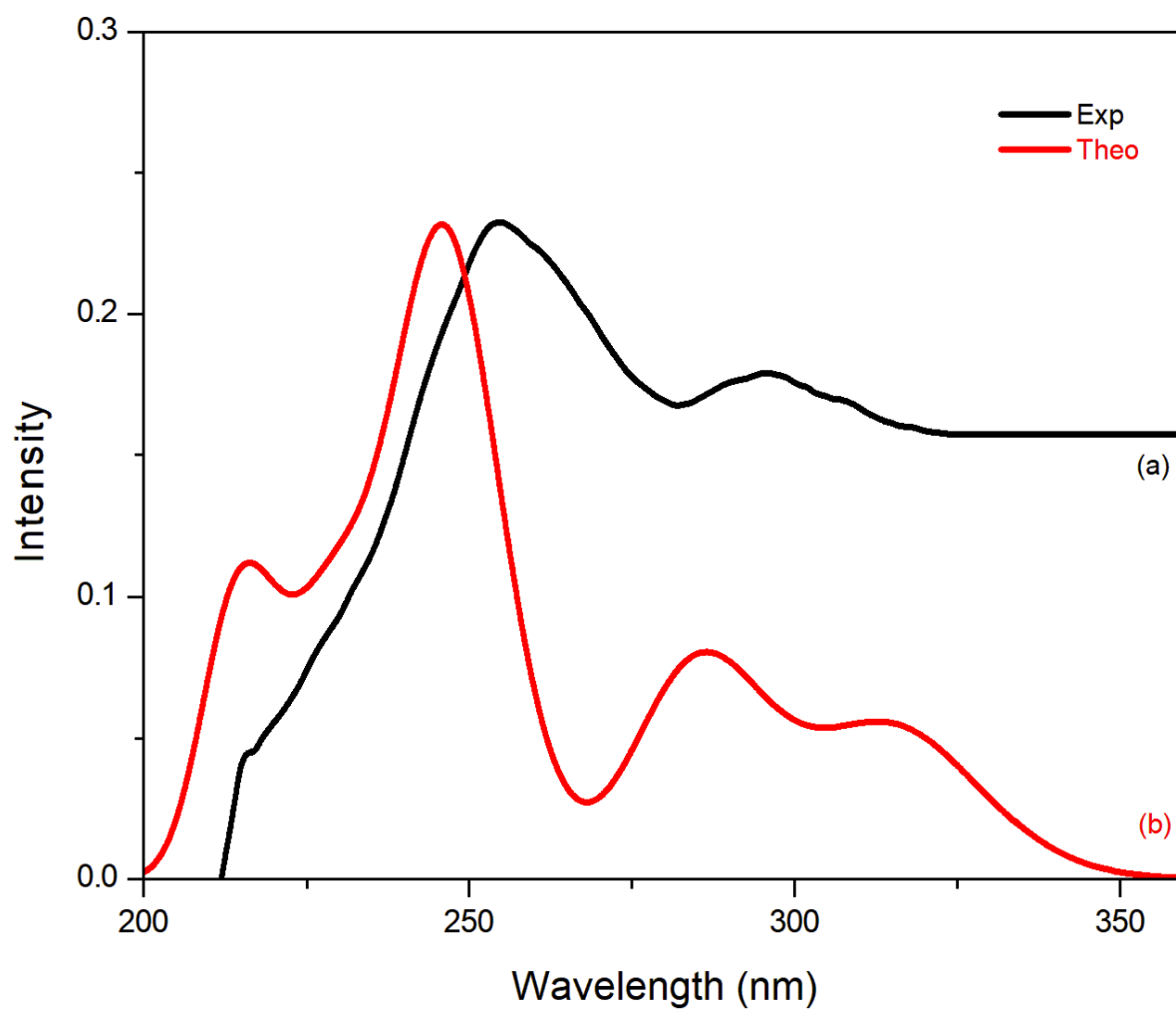


Fig. 6 (a) Experimental and (b) computed UV-visible spectra of the compound.

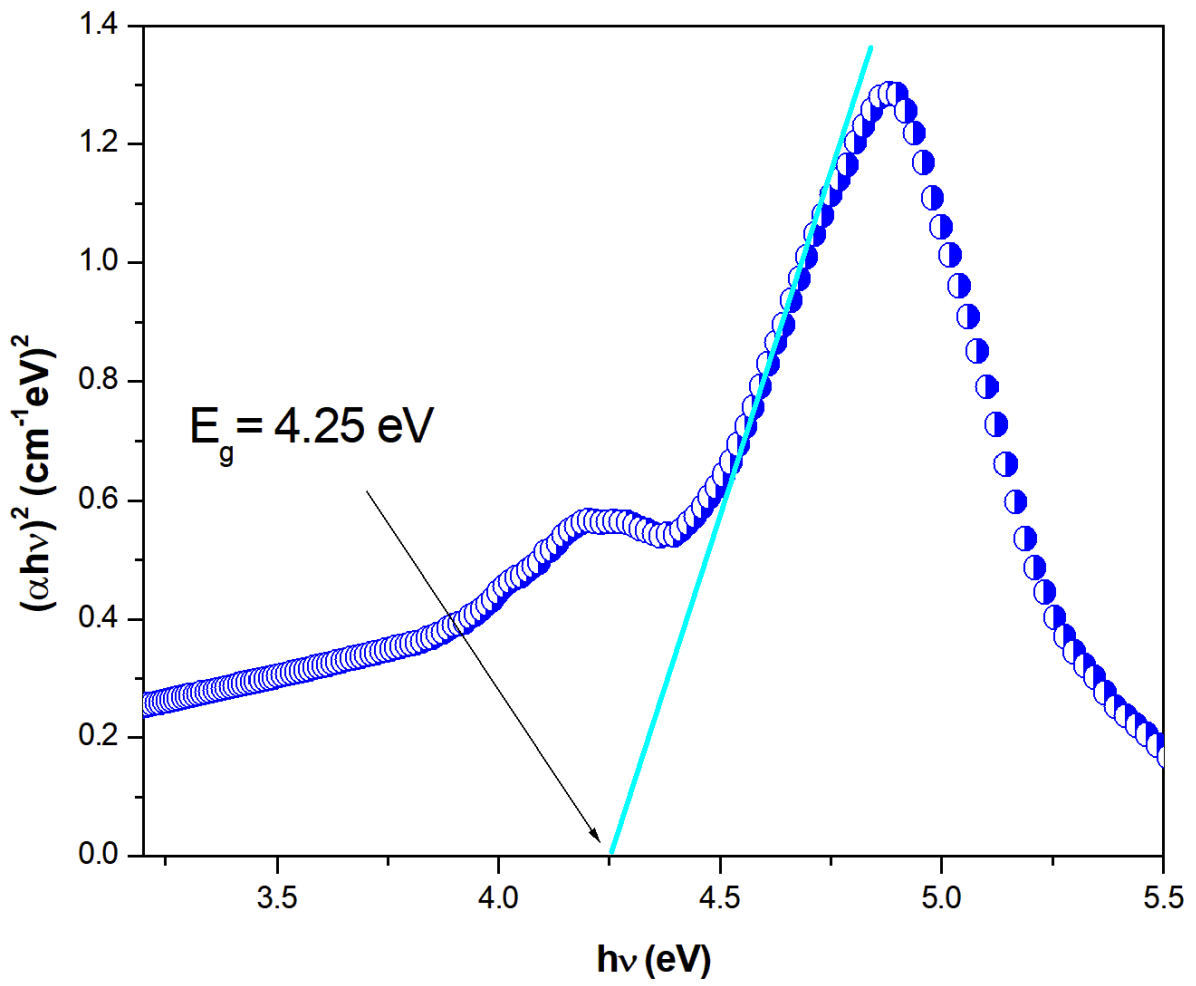


Fig. 7 Energy gap of $(\text{C}_{10}\text{N}_4\text{H}_{28})[\text{Cd}_3\text{Cl}_{10}(\text{H}_2\text{O})]\cdot\text{H}_2\text{O}$ determined by Tauc model.

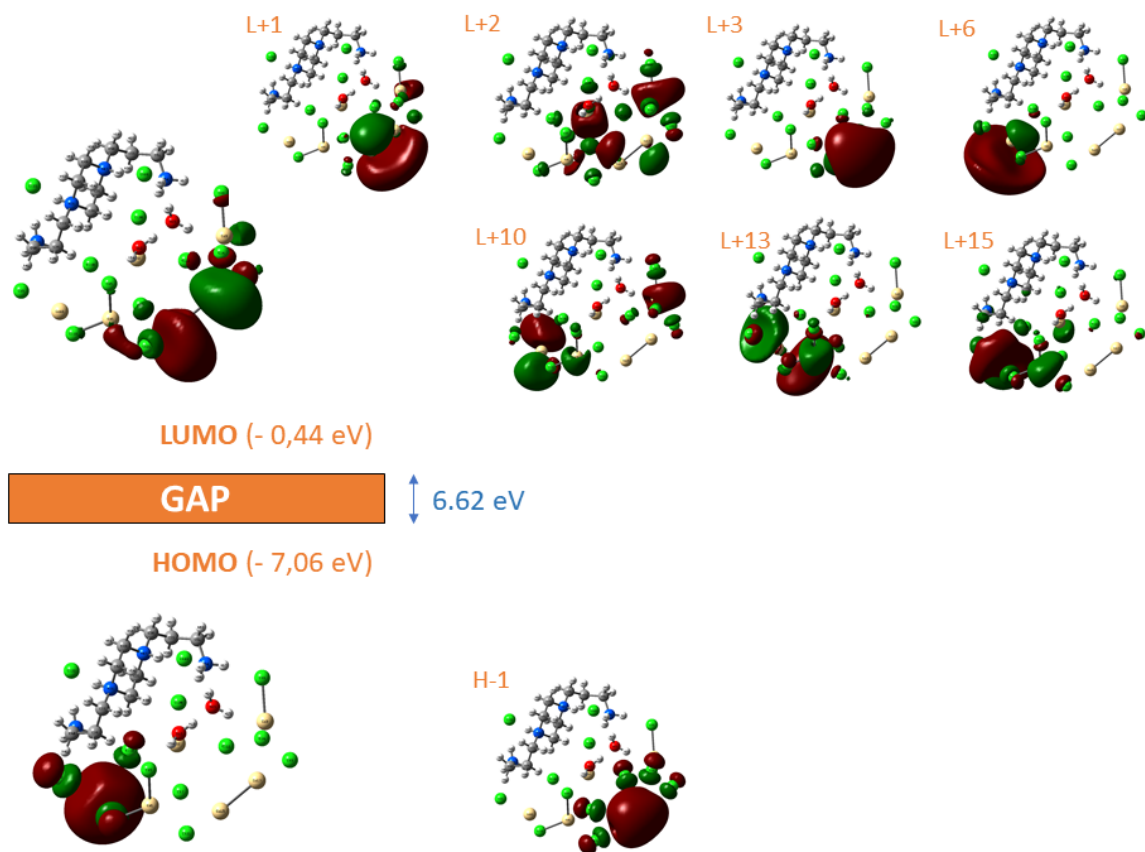


Fig. 8 Orbital frontier representation and energy of some molecular orbitals calculated using TDDFT theory

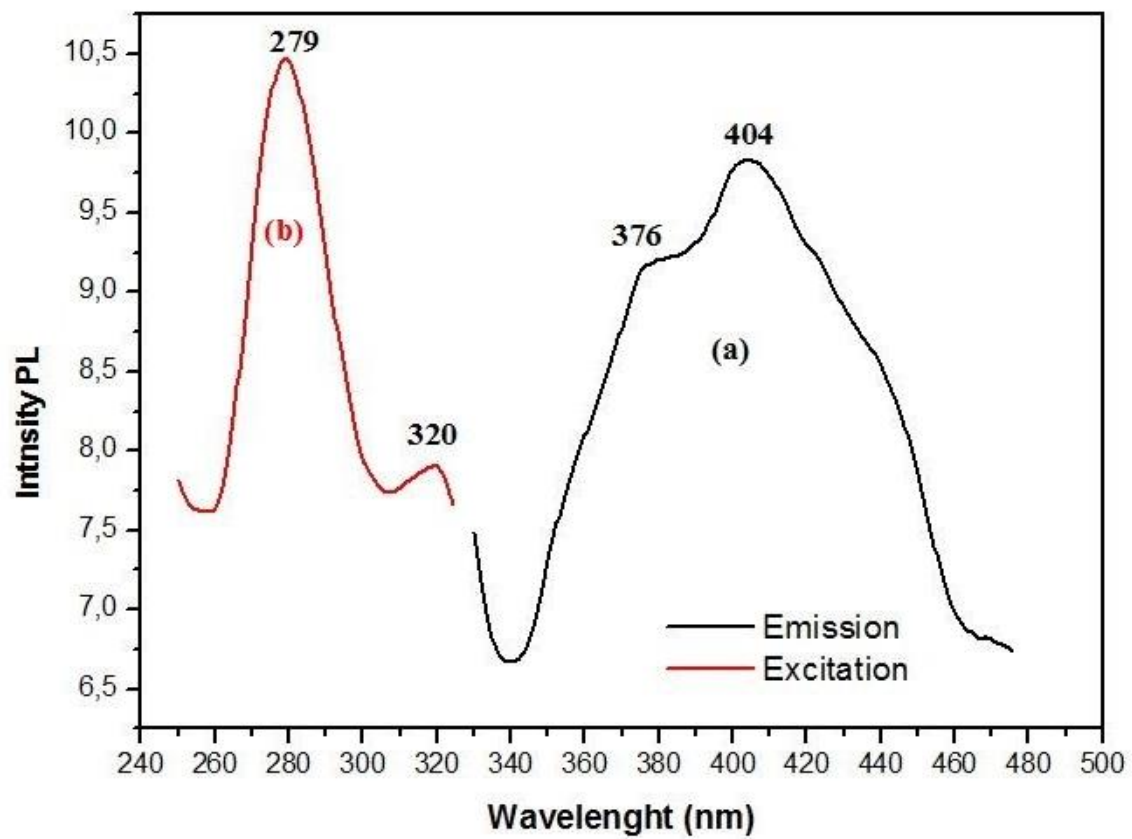


Fig. 9 Photoluminescent spectrum of $(C_{10}N_4H_{28})[Cd_3Cl_{10}(H_2O)] \cdot H_2O$.

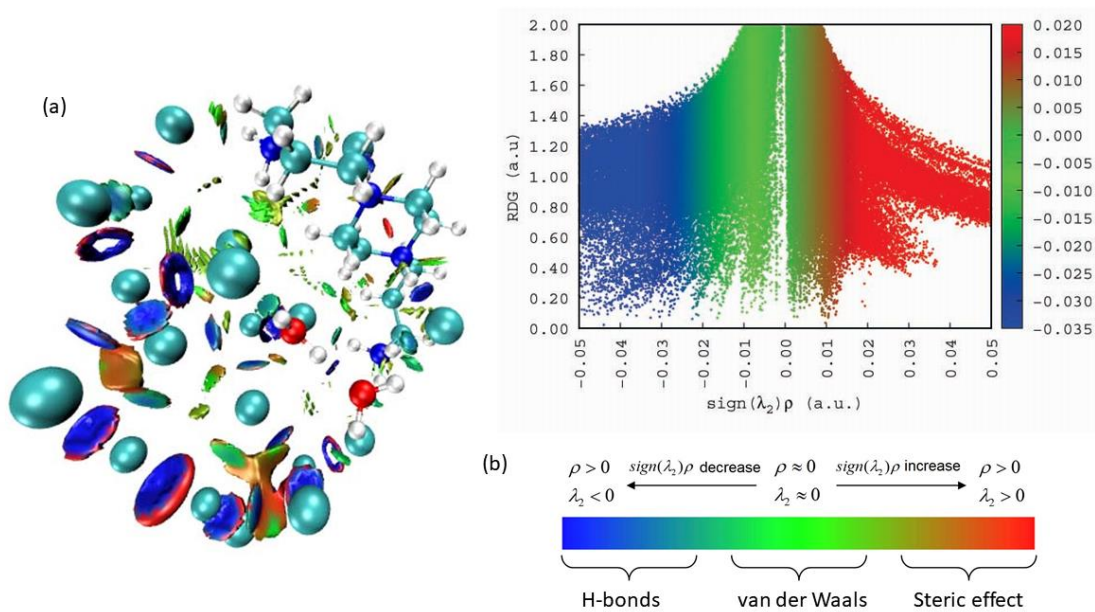


Fig 10. The plot of reduced density gradient (RDG) scatter (a), and the color filled isosurface of the compound (b).

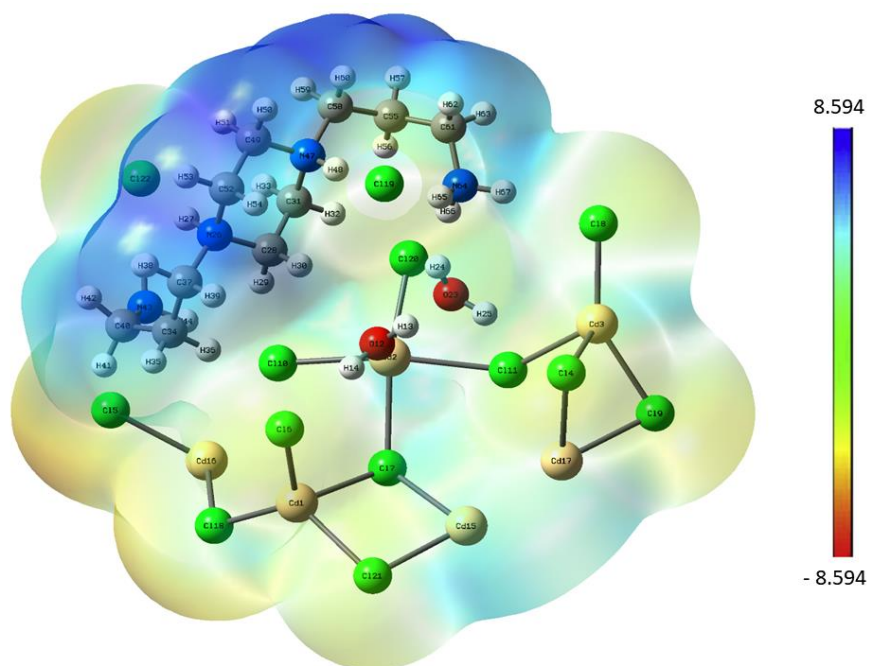


Fig. 11 Molecular electrostatic potential surface of $(C_{10}N_4H_{28})[Cd_3Cl_{10}(H_2O)] \cdot H_2O$.

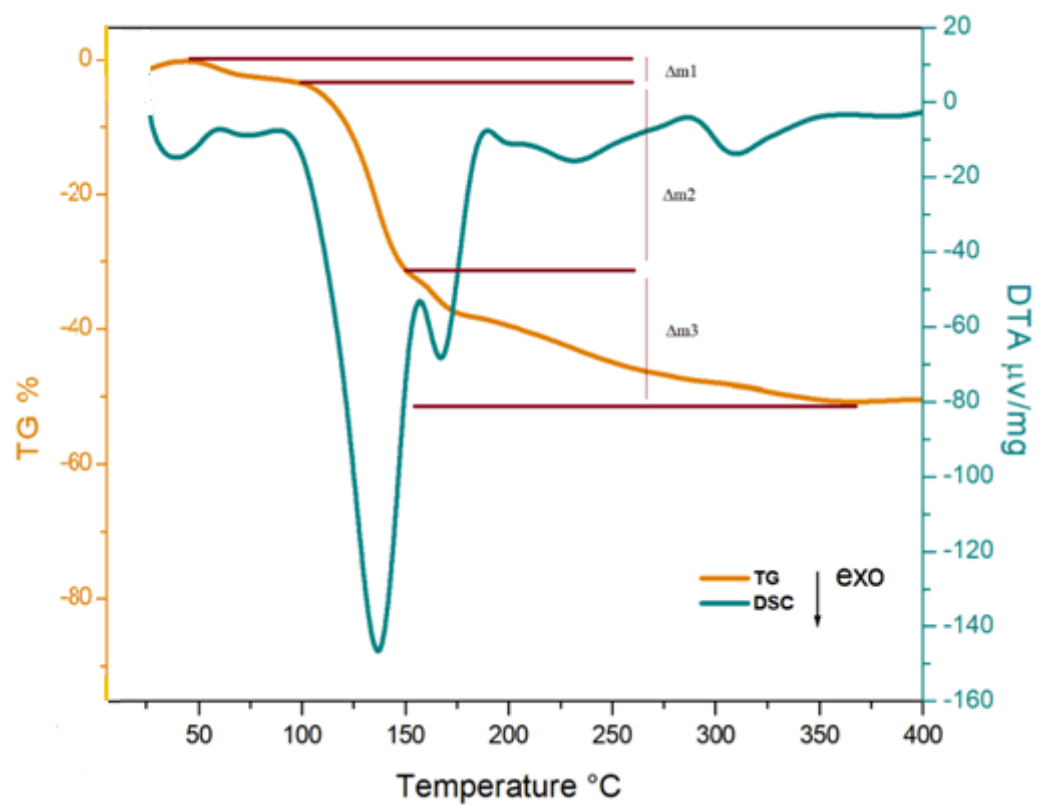


Fig. 12 TG-DTA curves of $(C_{10}N_4H_{28})[Cd_3Cl_{10}(H_2O)] \cdot H_2O$.

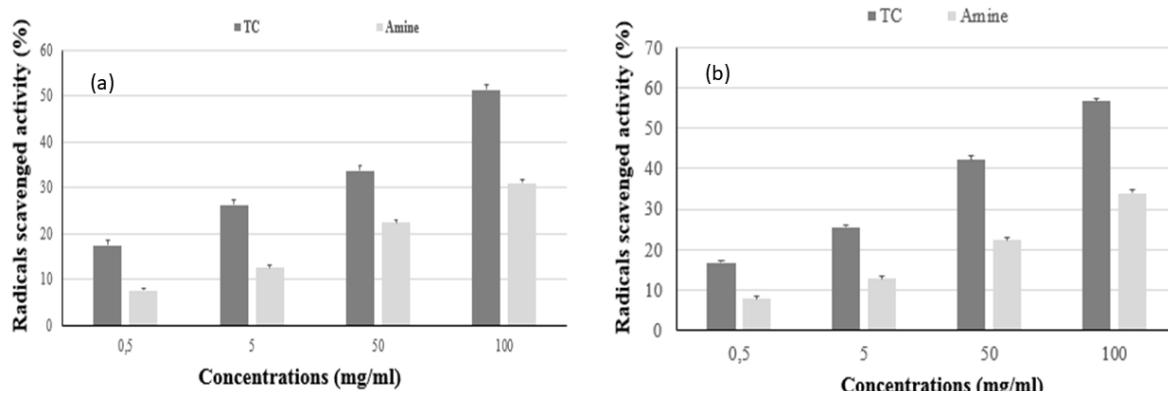


Fig. 13 (a) Scavenging activity of the title compound (TC) and the amine in DPPH test. (b) Scavenging activity of the title compound (TC) and the amine in ABTS test. The data are reported as mean \pm standard deviation.

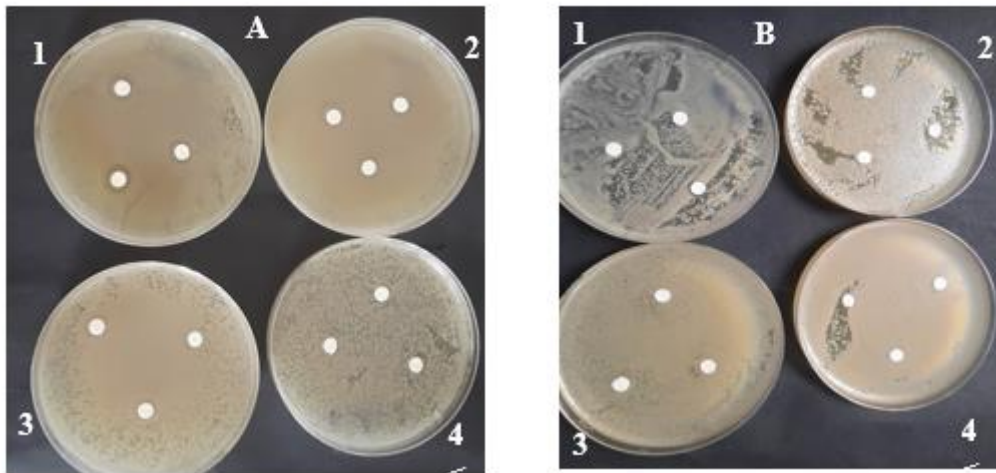


Fig. 14 Zone of inhibition (mm), caused by the title compound (TC) and the amine against bacteria: **1:** *Staphylococcus aureus* **2:** *Escherichia coli*, **3:** *Pseudomonas aeruginosa* , **4:** *Salmonella typhimurium*.**A:** TC, **B:** Amine.

Table 1 Crystallographic data and structure refinement parameters of $(C_{10}N_4H_{28})[Cd_3Cl_{10}(H_2O)] \cdot H_2O$.

<i>Crystal data</i>	
Chemical formula	$Cd_3Cl_8H_2O \cdot H_2O \cdot C_5H_{14}N_2$
M_r	759.01
Crystal system, space group	$P2_1/n$
Temperature (K)	150
a, b, c (Å)	10.7131(12), 13.1484(15), 14.0009(16)
β (°)	97.348(4)
V (Å³)	1956.0(4)
Z	4
Density (Mg.m⁻³)	2.577
μ (mm⁻¹)	4.32
Crystal size (mm³)	0.08 × 0.06 × 0.06
F(000)	1432
<i>Data collection</i>	
T_{min}, T_{max}	0.479, 0.691
No. of measured, independent and observed [$I > 2\sigma(I)$] reflections	40192 / 5986 / 5380
R_{int}	0.061
$(\Delta/\sigma)_{max}$	0.002
<i>Refinement</i>	
$R[F^2 > 2\sigma(F^2)], wR(F^2), S$	0.037, 0.105, 1.05
No. of reflections	5986
No. of parameters	186
No. of restraints	0
$\Delta\rho_{min}, \Delta\rho_{max}$ (e Å⁻³)	-2.37 < $\Delta\rho$ < 2.95

Table 2 Selected bond distances (Å) and angles (°) in (C₁₀N₄H₂₈)[Cd₃Cl₁₀(H₂O)].H₂O.

Distances (Å)			
Cd2—Cl2i	2.6794 (7)	Cl2—Cd2i	2.6795 (7)
Cd2—Cl8	2.6013 (7)	Cl2—Cd02iv	2.6912 (7)
Cd2—Cl5	2.6109 (7)	Cl8—Cd02v	2.6266 (7)
Cd2—Cl6	2.6482 (7)	Cl6—Cd2i	2.6575 (7)
Cd2—Cl6i	2.6575 (7)	Cl1—Cd02iv	2.5999 (7)
Cd2—Cl7	2.5511 (7)	O1—H1F	0.9389
Cd02—Cl2ii	2.6912 (7)	O1—H1G	0.9372
Cd02—Cl8iii	2.6266 (7)	N2—C3	1.487 (3)
Cd02—Cl1ii	2.5999 (7)	N2—C4vi	1.492 (3)
Cd02—Cl7	2.5637 (7)	N2—C2	1.506 (4)
Cd02—Cl4	2.5890 (7)	C3—C4	1.508 (4)
Cd02—O1	2.386 (2)	C4—N2vi	1.492 (3)
Cd1—Cl2	2.6669 (7)	C0AA—C2	1.508 (4)
Cd1—Cl5	2.6453 (7)	C0AA—C1	1.517 (4)
Cd1—Cl6	2.7300 (7)	C1—N1	1.486 (4)
Cd1—Cl3	2.6058 (7)	O2—H2C	0.8696
Cd1—Cl1	2.5825 (7)	O2—H2D	0.8697
Cd1—Cl4	2.5546 (7)		
Angles (°)			
Cl8—Cd2—Cl2i	86.31 (2)	Cl3—Cd1—Cl5	87.40 (2)
Cl8—Cd2—Cl5	94.64 (2)	Cl1—Cd1—Cl5	170.77 (2)
Cl8—Cd2—Cl6i	89.70 (2)	Cl1—Cd1—Cl6	92.90 (2)
Cl8—Cd2—Cl6	174.22 (2)	Cl1—Cd1—Cl3	93.50 (2)
Cl5—Cd2—Cl2i	175.00 (2)	Cl4—Cd1—Cl2	171.24 (2)
Cl5—Cd2—Cl6i	91.05 (2)	Cl4—Cd1—Cl5	95.91 (2)
Cl5—Cd2—Cl6	88.23 (2)	Cl4—Cd1—Cl6	89.91 (2)
Cl6i—Cd2—Cl2i	84.04 (2)	Cl4—Cd1—Cl3	92.49 (3)
Cl6—Cd2—Cl2i	90.41 (2)	Cl4—Cd1—Cl1	93.23 (2)
Cl6—Cd2—Cl6i	85.22 (2)	Cd2i—Cl2—Cd02iv	91.96 (2)
Cl7—Cd2—Cl2i	91.84 (2)	Cd1—Cl2—Cd2i	97.02 (2)
Cl7—Cd2—Cl8	93.29 (2)	Cd1—Cl2—Cd02iv	95.98 (2)
Cl7—Cd2—Cl5	93.01 (2)	Cd2—Cl8—Cd02v	95.25 (2)
Cl7—Cd2—Cl6	91.57 (2)	Cd2—Cl5—Cd1	94.13 (2)
Cl7—Cd2—Cl6i	174.74 (2)	Cd2—Cl6—Cd2i	94.78 (2)
Cl8iii—Cd02—Cl2ii	85.57 (2)	Cd2—Cl6—Cd1	91.36 (2)
Cl1ii—Cd02—Cl2ii	81.42 (2)	Cd2i—Cl6—Cd1	96.03 (2)
Cl1ii—Cd02—Cl8iii	89.72 (2)	Cd1—Cl1—Cd02iv	100.39 (2)
Cl7—Cd02—Cl2ii	172.40 (2)	Cd2—Cl7—Cd02	129.65 (3)
Cl7—Cd02—Cl8iii	98.12 (2)	Cd1—Cl4—Cd02	127.29 (3)
Cl7—Cd02—Cl1ii	91.91 (2)	Cd02—O1—H1F	112.7
Cl7—Cd02—Cl4	97.22 (2)	Cd02—O1—H1G	112.2
Cl4—Cd02—Cl2ii	89.21 (2)	Cl3—Cd1—Cl6	173.03 (2)
Cl4—Cd02—Cl8iii	92.83 (2)	Cl1—Cd1—Cl2	82.21 (2)
Cl4—Cd02—Cl1ii	170.08 (2)	C3—N2—C4vi	109.1 (2)
O1—Cd02—Cl2ii	96.64 (5)	C3—N2—C2	113.3 (2)
O1—Cd02—Cl8iii	177.09 (5)	C4vi—N2—C2	110.2 (2)
O1—Cd02—Cl1ii	92.48 (5)	N2—C3—C4	111.7 (2)
O1—Cd02—Cl7	79.92 (5)	N2vi—C4—C3	111.9 (2)
O1—Cd02—Cl4	85.32 (5)	C2—C0AA—C1	110.1 (2)

C12—Cd1—Cl6	82.89 (2)	N2—C2—C0AA	112.4 (2)
C15—Cd1—Cl2	88.56 (2)	N1—C1—C0AA	109.3 (2)
C15—Cd1—Cl6	85.84 (2)	H1F—O1—H1G	101.2
C13—Cd1—Cl2	95.24 (2)	H2C—O2—H2D	109.5

Symmetry codes: (i) $-x, -y+1, -z+1$; (ii) $x+1/2, -y+3/2, z+1/2$; (iii) $-x+1/2, y+1/2, -z+3/2$; (iv) $x-1/2, -y+3/2, z-1/2$; (v) $-x+1/2, y-1/2, -z+3/2$; (vi) $-x+2, -y+1, -z+2$.

Table 3 Hydrogen bonding parameters ($\text{\AA}, ^\circ$) of $(\text{C}_{10}\text{N}_4\text{H}_{28})[\text{Cd}_3\text{Cl}_{10}(\text{H}_2\text{O})]\cdot\text{H}_2\text{O}$.

<i>D—H</i> ⋯ <i>A</i>	<i>D—H</i>	<i>H</i> ⋯ <i>A</i>	<i>D</i> ⋯ <i>A</i>	<i>D—H</i> ⋯ <i>A</i>
O1—H1F ⋯ O2	0.940	1.753	2.637	155.63
O1—H1G ⋯ Cl5	0.937	2.394	3.271	155.75
N1—H1D ⋯ O1	0.910	2.014	2.922	175.24
N1—H1E ⋯ Cl8	0.910	2.349	3.192	154.04
O2—H2C ⋯ Cl3	0.869	2.340	3.182	162.88
N2—H2 ⋯ Cl3	1.000	2.252	3.192	156.22
C4—H4B ⋯ Cl3	0.989	2.929	3.677	133.18
C4—H4A ⋯ Cl7	0.990	2.509	3.371	145.33
O2—H2D ⋯ Cl6	0.869	2.649	3.410	146.87
N1—H1C ⋯ Cl3	0.910	2.435	3.258	150.63
C2—H2B ⋯ O2	0.990	2.621	3.395	135.08
C2—H2A ⋯ Cl1	0.990	2.924	3.721	138.25
C2—H2B ⋯ Cl8	0.990	2.949	3.773	141.30

Table 4 Hirshfeld contact surfaces, derived random contacts and enrichment ratios of different species present on the molecular surface in the compound.

	Cl···H/ H···Cl	Cd···Cl/ Cl···Cd	H···H	Cl···Cl	O···H/ H···O	O···Cl/ Cl···O	Cd···H/ H···Cd
Major Contacts %	62	17	12.1	6.4	2.1	0.2	0.2
Random contacts%	40.71	7.91	19.58	21.16	1.01	1.05	7.61
Enrichment	1.52	2.14	0.61	0.3	2.07	0.19	0.02

Table 5 Experimental and theoretical infrared band characteristics.

<i>Experimental</i>	<i>Theoretical</i>	<i>Assignments</i>
3852	3930, 3530	ν_s OH
3609	3530	ν_a OH
3565	3644, 3471, 3568, 3511, 3570, 3187, 3251	ν_s NH
3435	3269	ν_a NH
3348-2751	3403, 3306, 3396, 3295, 3249, 3332, 3262, 3321, 3360, 3292, 3364, 3353, 3283, 3309, 3233, 3329, 3353	ν_s CH
3348-3161	3360, 3364, 3329, 3353	ν_a CH
1052	1127, 1203, 1208, 1229, 1173	ν_s CC
934	1187, 1027, 1014, 818	ν_s NC
1643	1658, 1637, 1641, 1662, 1648, 1639	δ_s HCH
1637	1668	δ_s HOH
1350	1384	δ_{as} HOH
1867	1827, 1789, 2170, 1841	δ HNH
1506	1501, 1681, 1687	δ_{as} HNC
1494	1430, 1392, 1523, 1448, 1518	δ_s HCC
1612	1559	δ_{as} HCC
1270	1384	τ HOHO
1426	1553, 918	τ HCCN
1469	1559, 1576	τ HCCC
660	524	δ_{as} CCN
	514	δ_s CCN
418	306, 434, 284	δ_s NCC
610	530, 631	δ_s CNC
517	524	δ_s CCC
	1866, 1841, 2170, 1789	δ_s HNH
747	799	δ_s CdOH
	264	τ NCCN
	58, 135, 81, 52, 146	δ_s ClCdCl
	301, 282, 260, 244, 229, 255, 213, 255, 205, 163	ν_s CdCl
	284	ν_s CdO

	169, 89	τ CdClCdCl
	87	τ ClCdClO

* v: stretching, τ : torsion δ : deformation, a: asymmetric, s: symmetric

Table 6 Experimental and computed UV-Vis. spectral parameters of the compound.

<i>Experimental λ (nm)</i>	<i>Calculated λ (nm)</i>	<i>Oscillator strength</i>	<i>Major Contribution*</i>	<i>Assignments</i>
307	315.358	0.2165	H \rightarrow L+6 (20%)	CTLTM
			H \rightarrow L+10 (21%)	CTMM + CTML
295	285.623	0.3251	H \rightarrow L+15 (20%)	CTML
254	250.876	0.2446	H \rightarrow L+13 (49%)	CTML
	244.919	0.7357	H-1 \rightarrow L (41%)	CTML + CTMM
	233.864	0.0089	H \rightarrow L (20%),	CTMM
			H \rightarrow L+2 (23%)	CTML + CTMM
	229.356	0.3754	H-1 \rightarrow L+1 (35%)	CTML
215	214.853	0.4318	H-1 \rightarrow L+3 (34%)	CTLTM

* Only orbital percentages larger than 20% are reported; H: HOMO; L: LUMO

Table 7 Calculated HOMO and LUMO energy values and other related parameters of the compound.

Parameters	Values (eV)
E_{HOMO}	-7.06
E_{LUMO}	-0.44
Energy band gap $ E_{\text{HOMO}}-E_{\text{LUMO}} $	6.62
Chemical hardness $\eta = \frac{(I-A)}{2}$	3.31
Chemical potential for the molecule $\mu = \frac{-(I+A)}{2}$	-3.75
The softness $S = \frac{1}{2\eta}$	0.15
Electrophilicity index of the molecule $W = \frac{\mu^2}{2\eta}$	2.12
Electronegativity $\chi = \frac{(I+A)}{2}$	3.75

Table 8 Important second-order perturbation energies E(2) (donor→acceptor).

Donor NBO(i)	Acceptor NBO(j)	E ⁽²⁾ Kcal/mol	E(j)-E(i) (a.u)	F(i,j) (a.u)
LP ₍₃₎ C16	BD* ₍₁₎ O12 - H14	7.33	1.22	0.120
LP ₍₃₎ C118	LP* ₍₈₎ Cd16	8.18	0.81	0.103
LP ₍₃₎ C19	BD* ₍₁₎ Cd3 -C19	6.95	0.78	0.093
BD ₍₁₎ Cd3 -C19	LP* ₍₆₎ Cd17	28.46	1.18	0.239
LP ₍₃₎ C19	LP* ₍₆₎ Cd17	17.67	0.82	0.154
LP ₍₃₎ C19	LP* ₍₇₎ Cd17	6.78	0.64	0.084
LP ₍₃₎ C18	BD* ₍₁₎ N64 - H67	6.06	1.17	0.107
LP ₍₄₎ C14	LP* ₍₆₎ Cd3	25.89	0.94	0.198
LP ₍₄₎ C14	LP* ₍₇₎ Cd3	9.84	0.90	0.121
LP ₍₄₎ C14	BD* ₍₁₎ Cd3 -C19	9.80	1.03	0.129
LP ₍₃₎ C14	LP* ₍₆₎ Cd17	7.84	0.83	0.104
LP ₍₃₎ C14	LP* ₍₇₎ Cd17	9.73	0.64	0.100
LP ₍₄₎ C14	LP* ₍₆₎ Cd17	9.11	1.07	0.125
LP ₍₂₎ C14	BD* ₍₁₎ O23 - H25	3.60	1.25	0.085
LP ₍₄₎ C15	LP* ₍₇₎ Cd16	25.14	0.80	0.180
LP ₍₃₎ C15	BD* ₍₁₎ N43 - H46	5.81	1.15	0.104
LP ₍₄₎ C17	LP* ₍₆₎ Cd1	19.28	0.94	0.172
LP ₍₄₎ C17	LP* ₍₇₎ Cd1	16.49	0.91	0.155
LP ₍₃₎ C17	LP* ₍₆₎ Cd2	14.75	0.70	0.136
LP ₍₃₎ C17	LP* ₍₇₎ Cd2	18.14	0.97	0.169
LP ₍₃₎ C17	LP* ₍₈₎ Cd2	10.97	0.95	0.130
LP ₍₂₎ C17	LP* ₍₇₎ Cd15	8.74	0.77	0.104
LP ₍₂₎ C110	LP* ₍₈₎ Cd2	5.48	1.27	0.109
LP ₍₄₎ C110	LP* ₍₆₎ Cd2	25.99	0.66	0.174
LP ₍₄₎ C110	LP* ₍₇₎ Cd2	14.57	0.93	0.147
LP ₍₄₎ C110	LP* ₍₈₎ Cd2	16.89	0.91	0.157
LP ₍₂₎ C110	BD* ₍₁₎ N43 - H44	3.14	1.65	0.091
LP ₍₃₎ C111	LP* ₍₆₎ Cd2	8.05	1.06	0.124
LP ₍₃₎ C111	LP* ₍₇₎ Cd2	6.26	1.33	0.117
LP ₍₃₎ C111	LP* ₍₈₎ Cd2	19.15	1.31	0.203
LP ₍₃₎ C111	LP* ₍₆₎ Cd3	5.70	1.25	0.108
LP ₍₃₎ C111	LP* ₍₇₎ Cd3	5.69	1.21	0.105
LP ₍₄₎ C111	LP* ₍₆₎ Cd3	16.22	0.74	0.138
LP ₍₄₎ C111	LP* ₍₇₎ Cd3	17.05	0.70	0.139
LP ₍₄₎ C111	BD* ₍₁₎ Cd3 -C19	9.60	0.82	0.114
LP ₍₂₎ C111	LP* ₍₈₎ Cd17	7.28	0.64	0.086
BD ₍₁₎ O12 - H13	LP* ₍₉₎ Cd2	4.25	1.29	0.096
BD ₍₁₎ O12 - H14	LP* ₍₉₎ Cd2	4.12	1.27	0.094
LP ₍₂₎ O12	LP* ₍₆₎ Cd2	16.53	0.82	0.158
LP ₍₂₎ O12	LP* ₍₉₎ Cd2	20.04	0.99	0.179
LP ₍₃₎ C119	BD* ₍₁₎ O23 - H24	3.08	1.20	0.077
LP ₍₃₎ C119	BD* ₍₁₎ N64 - H65	5.58	1.09	0.099
LP ₍₄₎ C119	BD* ₍₁₎ N47 - H48	20.26	1.08	0.188
LP ₍₄₎ C119	BD* ₍₁₎ N64 - H65	2.51	1.15	0.069
LP ₍₁₎ C120	LP* ₍₇₎ Cd2	6.86	1.24	0.121
LP ₍₄₎ C120	LP* ₍₆₎ Cd2	33.23	0.71	0.203
LP ₍₄₎ C120	LP* ₍₇₎ Cd2	26.12	0.98	0.203
LP ₍₄₎ C120	LP* ₍₈₎ Cd2	7.04	0.96	0.105
LP ₍₃₎ C120	BD* ₍₁₎ N64 - H66	7.96	1.18	0.123
LP ₍₃₎ C121	LP* ₍₆₎ Cd1	4.44	0.68	0.070
LP ₍₄₎ C121	LP* ₍₆₎ Cd1	28.45	1.06	0.221

LP ⁽⁴⁾ C121	LP* ⁽⁷⁾ Cd1	4.84	1.03	0.090
LP ⁽¹⁾ C121	LP* ⁽⁶⁾ Cd15	5.01	1.26	0.104
LP ⁽³⁾ C121	LP* ⁽⁶⁾ Cd15	13.96	0.81	0.135
LP ⁽⁴⁾ C121	LP* ⁽⁶⁾ Cd15	18.59	1.20	0.190
LP ⁽³⁾ C122	BD* ⁽¹⁾ N43 - H45	7.60	1.06	0.113
LP ⁽⁴⁾ C122	BD* ⁽¹⁾ N26 - H27	22.67	1.07	0.197
LP ⁽⁴⁾ C122	BD* ⁽¹⁾ N43 - H45	2.88	1.16	0.074
LP ⁽²⁾ O23	BD* ⁽¹⁾ O12 - H13	19.61	1.52	0.218

LP: lone pair

BD: 2-center bond

E⁽²⁾: Stabilization energy

E(i)-E(j): Energy difference between the donor and acceptor NBO orbitals

F(i,j): The Fock Matrix element between i and j NBO orbitals

Table 9 NBO results showing the formation of Lewis and non-Lewis orbital in $(C_{10}N_4H_{28})[Cd_3Cl_{10}(H_2O)].H_2O$

Bond A-B	Occupation	EDA (%)	EDB (%)	NBO
BD ₍₁₎ O12 - H14	0.99806	78.04	21.96	0.8834* O 12 s(30.80%)p 2.25(69.20%) 0.4686* H 14 s(100.00%)
BD* ₍₁₎ Cd 3 -Cl 9	0.06001	92.05	7.95	0.9594*Cd 3 s(40.97%)p 1.43(58.76%)d 0.01(0.27%) -0.2820*Cl 9 s(37.11%)p 1.69(62.89%)
BD* ₍₁₎ N64 - H67	0.01387	25.05	74.95	0.5005* N 64 s(23.49%)p 3.26(76.51%) -0.8657* H 67 s(100.00%)
BD* ₍₁₎ O23 - H25	0.00764	22.70	77.30	0.4765* O 23 s(29.68%)p 2.37(70.32%) -0.8792* H 25 s(100.00%)
BD* ₍₁₎ N43 - H46	0.01501	24.70	75.30	0.4970* N 43 s(23.66%)p 3.23(76.34%) -0.8677* H 46 s(100.00%)
BD* ₍₁₎ N43 - H44	0.01340	25.99	74.01	0.5098* N 43 s(23.58%)p 3.24(76.42%)
BD* ₍₁₎ Cd15 -Cd17	0.99937	51.92	48.08	0.7206*Cd 15 s(83.31%)p 0.19(16.07%)d 0.01(0.62%) 0.6934*Cd 17 s(78.47%)p 0.27(21.14%)d 0.01(0.40%)
BD* ₍₁₎ O23 - H24	0.99965	77.37	22.63	0.8796* O 23 s(29.58%)p 2.38(70.42%) 0.4757* H 24 s(100.00%)
BD* ₍₁₎ N64 - H65	0.99585	74.79	25.21	0.8648* N 64 s(24.50%)p 3.08(75.50%) 0.5021* H 65 s(100.00%)
BD* ₍₁₎ N47 - H48	0.98896	77.33	22.67	0.8794* N 47 s(23.32%)p 3.29(76.68%) 0.4761* H 48 s(100.00%)
BD* ₍₁₎ N64 - H66	0.01913	25.27	74.73	0.5026* N 64 s(24.37%)p 3.10(75.63%) -0.8645* H 66 s(100.00%)
BD* ₍₁₎ N26 - H27	0.05238	22.22	77.78	0.4714* N 26 s(23.37%)p 3.28(76.63%) -0.8819* H 27 s(100.00%)
BD* ₍₁₎ N43 - H45	0.02288	25.00	75.00	0.5000* N 43 s(25.36%)p 2.94(74.64%) -0.8660* H 45 s(100.00%)
BD* ₍₁₎ O12 - H13	0.99812	80.52	19.48	0.8973* O 12 s(35.64%)p 1.81(64.36%) 0.4413* H 13 s(100.00%)
LP ₍₃₎ Cl 6	0.97578	-	-	s(6.56%)p 14.25(93.44%)
LP* ₍₆₎ Cd1	0.09709	-	-	s(14.30%)p 5.99(85.57%)d 0.01(0.13%)
LP* ₍₆₎ Cd 15	0.07175	-	-	s(15.76%)p 5.33(83.96%)d 0.02(0.29%)
LP ₍₃₎ Cl 18	0.96831	-	-	s(25.28%)p 2.96(74.72%)
LP* ₍₈₎ Cd 16	0.02923	-	-	s(0.21%)p99.99(99.32%)d 2.25(0.47%)
LP* ₍₆₎ Cd 17	0.09989	-	-	s(21.07%)p 3.74(78.81%)d 0.01(0.13%)
LP* ₍₆₎ Cd 3	0.08235	-	-	s(6.93%)p13.39(92.83%)d 0.03(0.23%)
LP* ₍₆₎ Cd 17	0.09989	-	-	s(21.07%)p 3.74(78.81%)d 0.01(0.13%)
LP* ₍₆₎ Cd 17	0.09989	-	-	s(21.07%)p 3.74(78.81%)d 0.01(0.13%)
LP ₍₃₎ Cl8	0.96831	-	-	s(25.28%)p 2.96(74.72%)
LP ₍₄₎ Cl4	0.90626	-	-	s(34.61%)p 1.89(65.39%)
LP* ₍₆₎ Cd3	0.08235	-	-	s(6.93%)p13.39(92.83%)d 0.03(0.23%)
LP* ₍₇₎ Cd3	0.06666	-	-	s(0.08%)p99.99(99.73%)d 2.55(0.19%)
LP ₍₂₎ Cl4	0.98402	-	-	s(5.19%)p18.25(94.81%)
LP ₍₄₎ Cl5	0.95274	-	-	s(29.30%)p 2.41(70.70%)

LP*(7) Cd16	0.05732	-	-	s(12.64%)p 6.89(87.04%)d 0.02(0.31%)
LP (3) Cl5	0.97884	-	-	s(10.74%)p 8.31(89.26%)
LP (4) Cl7	0.92586	-	-	s(31.45%)p 2.18(68.55%)
LP*(7) Cd1	0.06106	-	-	s(0.10%)p99.99(99.71%)d 1.99(0.20%)
LP (3) Cl7	0.93388	-	-	s(26.13%)p 2.83(73.87%)
LP*(6) Cd2	0.17446	-	-	s(99.09%)p 0.01(0.79%)d 0.00(0.12%)
LP*(7) Cd2	0.08318	-	-	s(0.13%)p99.99(99.75%)d 0.90(0.12%)
LP*(8) Cd2	0.07985	-	-	s(0.63%)p99.99(99.27%)d 0.14(0.09%)
LP (4) Cl10	0.91909	-	-	s(25.67%)p 2.90(74.33%)
LP (2) Cl10	0.98179	-	-	s(63.98%)p 0.56(36.02%)
LP (3) Cl11	0.94444	-	-	s(70.31%)p 0.42(29.69%)
LP (4) Cl11	0.91226	-	-	s(10.23%)p 8.77(89.77%)
LP (2) O12	0.96016	-	-	s(32.08%)p 2.12(67.92%)
LP*(9) Cd2	0.05060	-	-	s(0.46%)p99.99(99.31%)d 0.48(0.22%)
LP (3) Cl19	0.97802	-	-	s(4.90%)p19.40(95.10%)
LP (4) Cl20	0.90947	-	-	s(30.39%)p 2.29(69.61%)
LP (3) Cl20	0.97120	-	-	s(12.31%)p 7.12(87.69%)
LP (4) Cl21	0.91425	-	-	s(45.11%)p 1.22(54.89%)
LP (3) Cl21	0.92096	-	-	s(1.28%)p77.41(98.72%)
LP (3) Cl22	0.97745	-	-	s(1.58%)p62.36(98.42%)
LP (4) Cl22	0.94177	-	-	s(16.47%)p 5.07(83.53%)
LP (2) O23	0.97607	-	-	s(37.36%)p 1.68(62.64%)

Table 10 Inhibition zone (mm), caused by the title compound (TC) and the amine against bacteria. The data are reported as mean \pm standard deviation. * p <0.05, ** p <0.01 significantly different from the compound.

Bacteria	Inhibition Zone (mm)	
	TC	Amine
<i>Pseudomonas aeruginosa</i> SH 38	9.16 \pm 0.27 **	6
<i>Escherichia coli</i> JW 1772	6.83 \pm 0.27 *	6
<i>Salmonella typhimurium</i> ATCC14028	6	6
<i>Staphylococcus aureus</i> NCTC6571	10 \pm 0.33 **	6